Summer 2016

Debris Flow Fans in Yosemite Valley National Park, California

Evan Scott Enriquez
San Jose State University

DEBRIS FLOW FANS IN YOSEMITE VALLEY NATIONAL PARK, CALIFORNIA

A Thesis

Presented to

The Faculty of the Department of Geology

San José State University

In Partial Fulfillment

of the Requirements for the Degree

Master of Science

by

Evan S. Enriquez

August 2016

The Designated Thesis Committee Approves the Thesis Titled

DEBRIS FLOW FANS IN YOSEMITE VALLEY NATIONAL PARK, CALIFORNIA

by

Evan S. Enriquez

APPROVED FOR THE DEPARTMENT OF GEOLOGY

SAN JOSÉ STATE UNIVERSITY

August 2016

Dr. Emmanuel Gabet	Department of Geology
Dr. Robert Miller	Department of Geology
Dr. Paula Messina	Department of Geology

ABSTRACT

DEBRIS FLOW FANS IN YOSEMITE VALLEY NATIONAL PARK, CALIFORNIA

by Evan S. Enriquez

Formation of debris flow fans poses a potential hazard to the infrastructure and inhabitants of Yosemite Valley. Research was conducted on debris flow fans at three field sites in Yosemite Valley: Indian Creek, Eagle Creek, and Sentinel Creek. The study utilized a Trimble Pro XR Differential Global Positioning System (DGPS), Cosmogenic Berellium-10 (^{10}Be) dating, and debris flow volume measurements to better understand the spatial distribution, age, and magnitude of prehistoric debris flow deposits at each field site. It is hypothesized that all three fans were constructed quickly after the last glacial maximum (LGM), which is dated at 19.8 ka. It is also proposed that increased rainfall and sediment production during the LGM provided the necessary conditions for debris flow initiation in each catchment. Future debris flow initiation is contingent on channels being pre-loaded with sediment and above average rainfall. At the present time, the channels are loaded with debris, but future debris flow initiation seems unlikely to occur because the fans have been inactive for thousands of years. Debris flows only pose a significant hazard to Yosemite Valley, if and when, the optimum conditions are met.

ACKNOWLEDGMENTS

First, I would like to thank my wonderful finance Carissa Harris. The completion of this project wouldn't have been possible without your help and encouragement. Next, I would like to thank Dr. Manny Gabet for taking me on as a graduate student and for mentoring me throughout this project. In addition, I would like to thank Dr. Robert Miller and Dr. Paula Messina for their insightful comments at the end of this process, which helped put the final polish on the production of this manuscript. Last, I would like to give a shout out to my parents Jenifer Enriquez and Manuel Enriquez, for without them no of this would be possible. I would like to dedicate this thesis in loving memory of Manuel Enriquez.

TABLE OF CONTENTS

LIST OF FIGURES

Figure

LIST OF TABLES

Table

INTRODUCTION

In mountainous areas, people live and work on fans formed through the deposition of fluvial and debris flow sediments. In these areas, there is the potential for loss of life and damage to infrastructure. Yosemite Valley National Park is an example of a place where people live and have built on alluvial and debris flow fans. In Yosemite Valley, fans are located along the valley floor, positioned below ephemeral channels and large cliffs. Some of these fans are identified as debris flow fans because bouldery debris flow levees are deposited along their surfaces. Historical accounts of debris flows in Yosemite Valley indicate that flows are capable of transporting boulders into the valley (Wieczorek and Jäger, 1996). With over four million annual visitors and 1,133 structures in Yosemite Valley, debris flows are natural hazards that require mitigation (National Park Service, 2012). The fans chosen for this study are positioned at the lower end of Eagle Creek, Indian Creek, and Sentinel Creek. These streams are tributaries of the Merced River, located in Yosemite Valley (Fig. 1).

It is recognized that debris flows mobilize by at least three processes: shallow landslides, progressive sediment bulking, and "the fire hose effect" (Larsen et al., 2006). In Yosemite Valley, it is probable that debris flows have initiated primarily through progressive sediment bulking and the fire hose effect. Progressive sediment bulking is indicated by the presence of steep channels that flow into the valley. In addition, the fire hose effect may occur where waterfalls flow onto talus piles along the valley floor. Progressive sediment bulking commonly occurs in previously burned watersheds and along steep bedrock channels (Larsen et al., 2006; Gabet and Bookter, 2008).

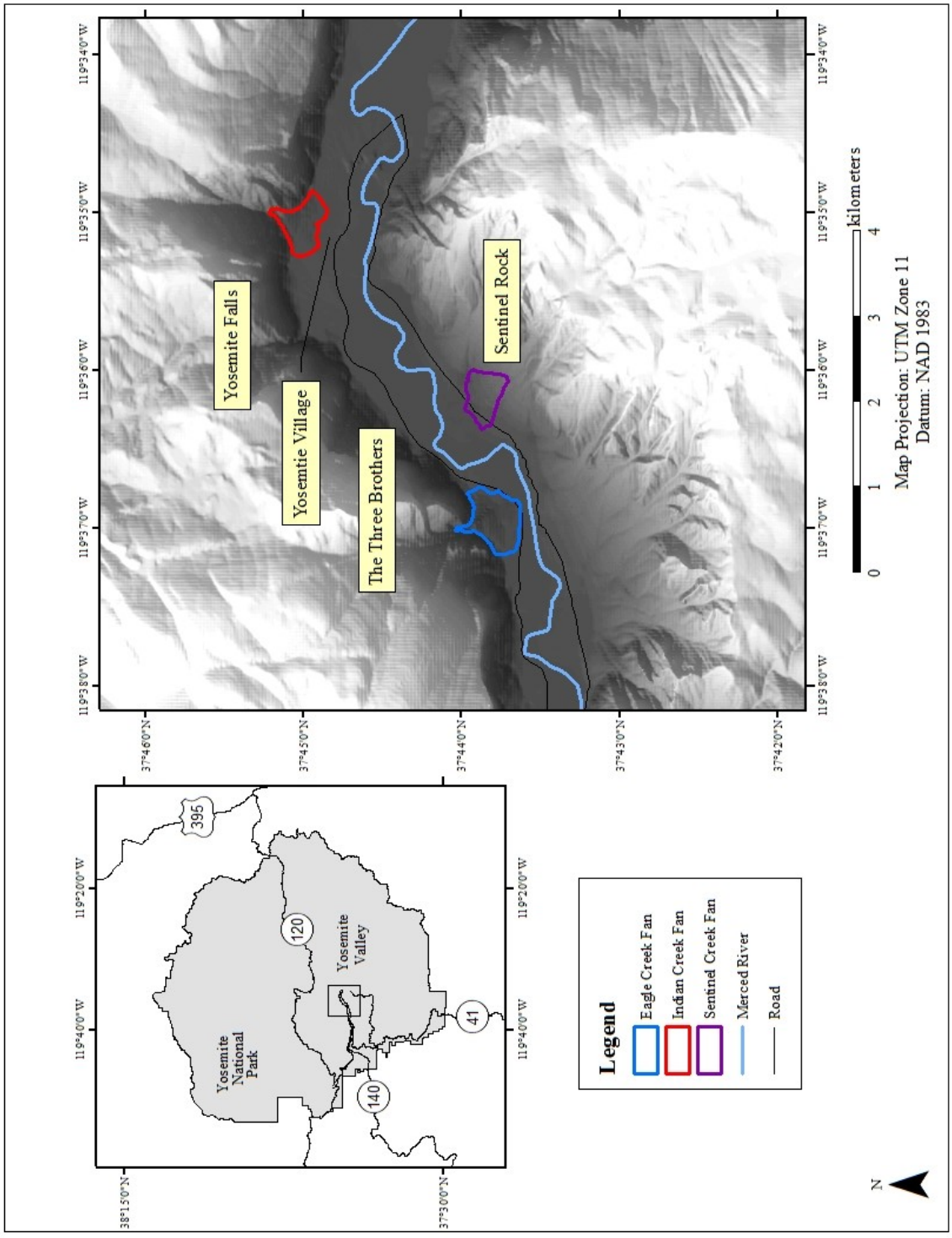

Figure 1. Map of study sites.

In these areas, decreased soil and bedrock infiltration can lead to overland flow. During a rainstorm, overland flow scours and entrains loose sediment along a channel network. Through time, sediment concentration increases dramatically, at which point, a debris flow forms when sufficient material has been incorporated (Larsen et al., 2006; Gabet and Bookter, 2008). Two requirements for progressive sediment bulking are: the presence of loose sediment, and high water discharge along a channel. This debris flow initiation process could apply to Eagle Creek and Indian Creek, which are steep, ephemeral channels that flow into Yosemite Valley. During a large rainstorm, material that has fallen into these channels by rock fall or dry ravel would be mobilized into a debris flow and deposited on the surface of both fans. The fire hose effect was first studied by Johnson and Rodine (1984), who observed debris flows at Karl Springs, in Death Valley National Park (California). In these events, debris flows are generated when water flows off a cliff at a high velocity, onto the top of a large talus pile (Johnson and Rodine, 1984). The force of the falling water causes sediment on the talus pile to disperse and mix with the flowing water. This interaction between the sediment and the water leads to the formation of a debris flow (Johnson and Rodine, 1984; Larsen et al., 2006). It is likely that the debris flows along Sentinel Creek have been initiated by the fire hose effect because the fan is positioned below a large talus pile and waterfall. During significant rainstorms, water flows off Sentinel Falls and initiates debris flows on the talus pile above the Sentinel Creek fan.

Fan deposition is controlled by debris flow rheology. Debris flow yield strength (eg., shear strength) is a controlling factor of debris flow rheology. Debris flows have

previously been described using a visco-plastic, or Bingham model. Debris flow deposition occurs when basal shear stress (τ_b) no longer exceeds debris flow yield strength (τ_o), or

$$\tau_b = \rho_b g d \sin\theta \leq \tau_o \quad (1)$$

$$\tau_o = \rho_b g d \sin\theta \quad (2)$$

where ρ_b is flow bulk density, g is gravity, d is flow depth, and θ is slope (Hooke 1967; Whipple and Dunne, 1992). Drops in basal shear stress can be related to decreases in fan slope and flow height. Two factors that control yield strength are sediment size and sediment concentration. Debris flows with high yield strength deposit fans with slopes of 4-5° and such flows are drier and have a greater percentage of coarse-grained sediment (Whipple and Dunne, 1992). The presence of coarse material intensifies grain boundary friction during the passage of a debris flow (Major and Iverson, 1999). Therefore, debris flows with high yield strength have shorter run out distances and deposit on steeper slopes. In contrast, debris flows with low yield strength deposit fans with slopes of about 1-2°. Debris flows that are wetter and contain a greater percentage of silt and clay have lower yield strength, which makes them more mobile due to decreased grain friction (Whipple and Dunne, 1992). The yield strength of debris flows has direct implications on fan construction in Yosemite Valley because fan morphology varies with sediment concentration and particle size.

Debris flow deposition occurs along the margins of a flow, where frictional resistance is highest (Schürch et al., 2011). During a debris flow, coarse-grained material moves to the flow front, forming a bouldery snout. The flow front becomes resistant to

movement due to increased grain friction. The coarse-grained material, located in the flow front, is pushed laterally by the advancing material behind it. The coarse-grained material is deposited along the flow margins as levees (Johnson et al., 2012).

The goal of this research was to assess the risk of debris flow hazards to the inhabitants and visitors of Yosemite Valley. This objective was accomplished by better understanding the frequency and magnitude of prehistoric debris flows. The identification and mapping of levees on the surface of each fan provided insight into the relative timing of debris flow deposition. Levees on the surface of each fan were paired together to distinguish individual flows, and cross-cutting relationships were used to order the flows from oldest to youngest. In a few instances, cosmogenic dating of levee boulders was employed to obtain absolute dates on individual debris flows. In addition, estimated flow volumes were used to understand how ancient debris flows compare to historic flows. If ancient flows were larger, then it is important to consider what environmental conditions produced them, and if the conditions are still present today. Last, this research has helped further the understanding of how debris flow fans are constructed.

Materials and Methods

Study Sites

Indian Creek, Eagle Creek, and Sentinel Creek are tributaries of the Merced River in Yosemite Valley, located in the central Sierra Nevada Mountains of California (Fig. 1). The Sierra Nevada is primarily composed of a Mesozoic-aged batholith (Bateman and Wahrhaftig, 1966). The Sierra Nevada Mountain range experienced uplift and tilting

during the Late Cretaceous to Early Paleogene (Bateman and Wahrhaftig, 1966). The crest of Yosemite Valley is at an elevation of 2700 meters, while the valley floor is at an elevation of 1100 m (National Center for Airborne Laser Mapping, 2006). The mean annual precipitation is 95.2 cm/year, which falls primarily as rain during the colder months of November through April (National Oceanic and Atmospheric Association, 2012). A snow pack develops at higher elevations (Wieczorek and Jäger, 1996). The current vegetation in the valley is composed of a mixed woodland forest and yellow pine forest (Anderson and Carpenter, 1991). Along the margins of the valley, alluvial and debris flow fans extend onto the valley floor (Wieczorek and Jäger, 1996). These deposits are assumed to postdate the last glacial maximum (LGM), the Tioga stage, which occurred between 28-14 ka in the Sierra Nevada (Rood et al., 2011). Cosmogenic dating of the Tioga terminal moraine in Yosemite Valley shows that glaciation peaked by approximately 19.8 ka. It is also estimated that the valley was ice free by about 16 ka (Stock and Uhrhammer, 2010).

This study investigated the debris flow fans deposited below the Indian Creek, Eagle Creek, and Sentinel Creek watersheds (Fig. 1). The Indian Creek fan is located on the northern side of Yosemite Valley, where Yosemite Village was built, and is approximately 630 m wide, with a maximum elevation of 1360 m. The bedrock of the Indian Creek watershed consists primarily of Sentinel and Half Dome Granodiorite (Calkins, 1985) (Fig. 2). The Eagle Creek fan is located on the northern side of Yosemite Valley, east of El Capitan, and is about 710 m wide, with a maximum elevation of 1361 m.

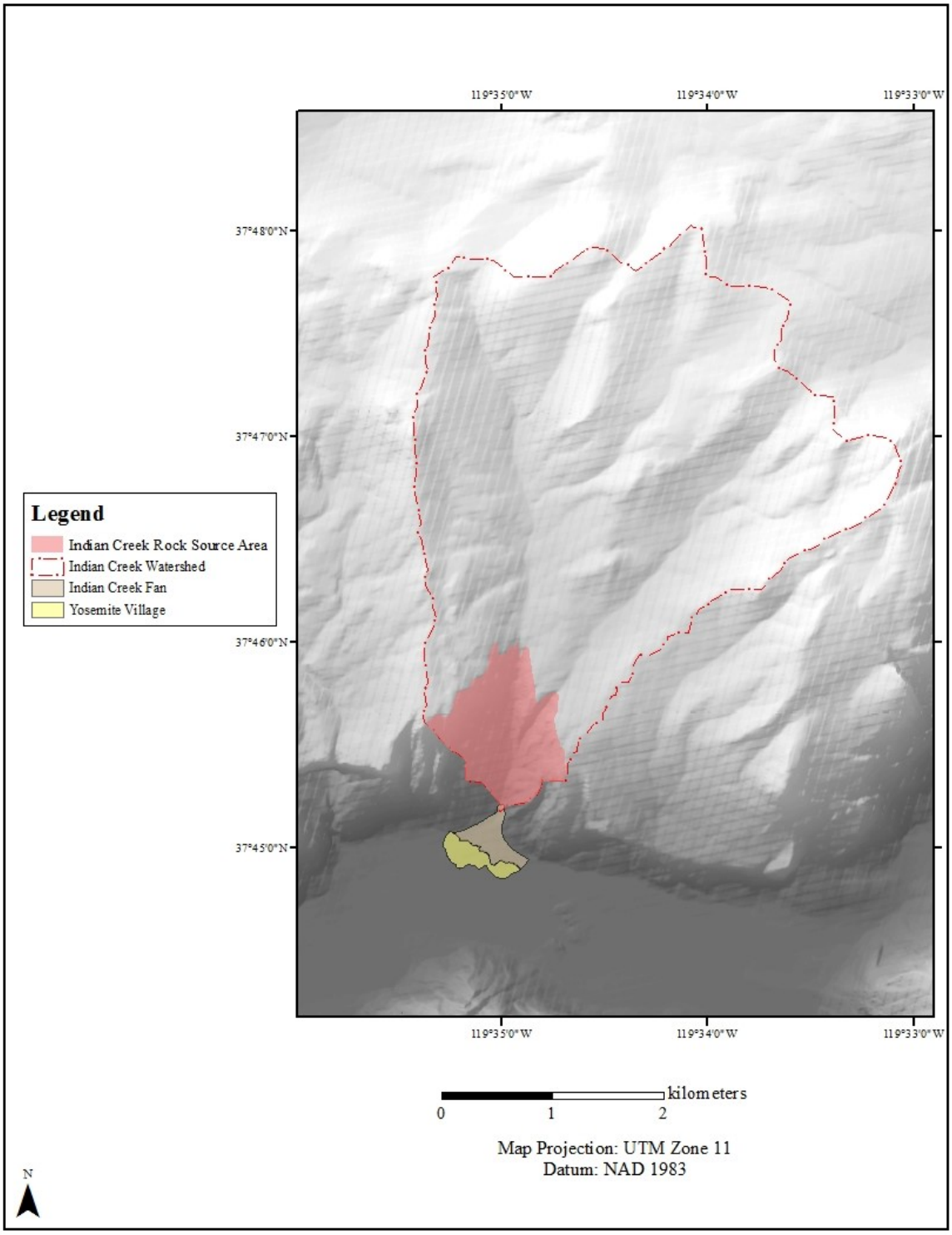

Figure 2. Map of the Indian Creek fan, watershed, and rock source area.

The bedrock of the Eagle Creek watershed consists primarily of El Capitan Granite (Calkins, 1985) (Fig. 3). The Sentinel Creek fan is located on the southern side of Yosemite Valley, positioned below Sentinel Falls, and is roughly 550 m wide, with a maximum elevation of 1326 m. The bedrock of the Sentinel Creek watershed consists primarily of Sentinel Granodiorite and small amounts of El Capitan Granite (Calkins, 1985) (Fig. 4).

The Sentinel Granodiorite has a uranium-lead (U-Pb) age of approximately 95 Ma (Bateman, 1992; Burgess et al., 2009). The unit is coarse-grained, dark in color, and contains well-formed crystals of hornblende, biotite, and sphene. The unit plots across the granite, granodiorite, and tonalite fields on a quartz - alkali feldspar - plagioclase feldspar (Q-A-P) diagram (Bateman, 1992). The Half Dome Granodiorite is the second oldest unit in the Tuolumne Intrusive Suite, with U-Pb ages of 92-89 Ma (Memeti et al., 2010). The unit contains an outer equigranular and inner megacrystic facies. The outer facie has been mapped south of Tuolumne along Indian Creek, which contains well-formed hornblende, biotite books, and titanite wedges. The unit plots primarily in the granodiorite field on a Q-A-P diagram (Bateman, 1992). The El Capitan Granite is the main unit of Yosemite Valley, with U-Pb ages of 102-103 Ma (Bateman, 1992). The unit contains abundant potassium feldspar, small biotite books, and little hornblende. The unit plots in the granite and granodiorite fields on a Q-A-P diagram (Bateman, 1992).

Mapping

Debris flow levees were mapped to understand the spatial distribution of debris flow events on the surface of each fan.

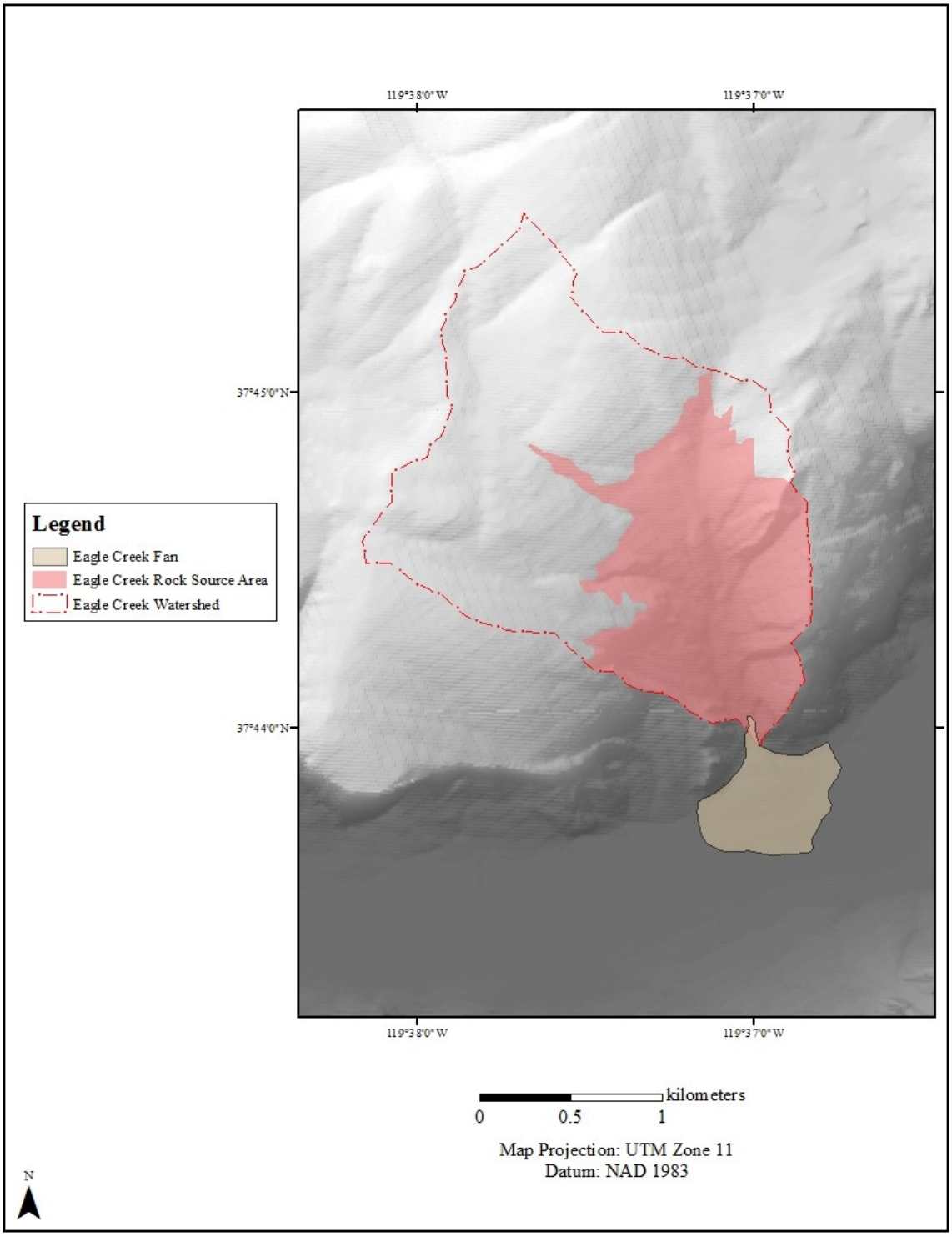

Figure 3. Map of the Eagle Creek fan, watershed, and rock source area.

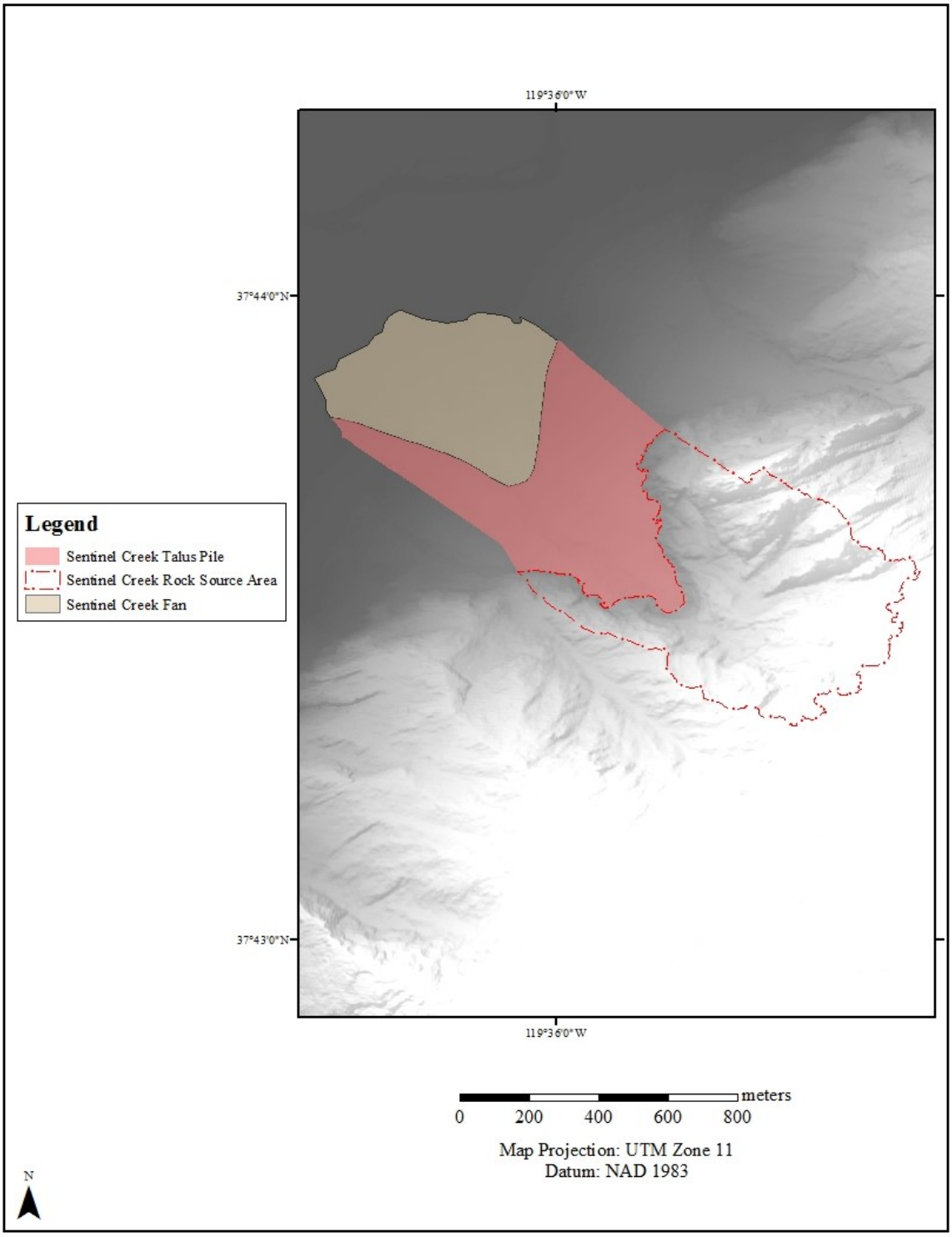

Figure 4. Map of the Sentinel Creek fan, rock source area, and talus pile.

Levees were identified in the field as rows of imbricated boulders that ranged in height from 1-3 m. In the field, debris flow levees were mapped with a Trimble Pro XR Differential Global Positioning System (DGPS) unit. In addition, waypoints were recorded at grain size measurement locations (see below). All DGPS data were post-processed using Trimble's Pathfinder software and then converted into geographical information system (GIS) feature classes. During post-processing, it was clear that some debris flow levees were missing from the DGPS data or they were overlooked during field work. Missing features were identified using a hill-shade relief model of the 2006 Yosemite Valley Light Detection and Ranging (LiDAR) dataset (National Center for Airborne Laser Mapping, 2006). Next, the missing debris flow levees were digitized using the ArcGIS editor toolbar.

Cosmogenic Dating

Cosmogenic Berellium-10 (^{10}Be) dating was used to determine the timing of debris flow deposition on the Indian Creek fan. Due to funding limitations, only five samples were collected from the top of the levees of the active channel on this fan. The samples were collected by the Yosemite National Park Geologist, Dr. Greg Stock. More than one sample was collected to protect against age inheritance and cosmic ray shielding. Age inheritance would cause sample ages to falsely imply older depositional ages, while cosmic ray shielding would imply samples ages to be younger. For instance, pre-deposition cosmic ray exposure would cause age inheritance. In contrast, boulder rotation and snow/vegetation shielding would cause samples to appear younger (Stock and Uhrhammer, 2010; Hidy et al., 2013). To minimize the risk of age inheritance and

cosmic ray shielding, samples were collected from large, stable boulders at the crest of each debris flow levee.

Grain Size Measurements of Debris Flow Levees

Grain size measurements were collected at the start and end of each levee. These measurements were used to understand how sediment size varies across the surface of each fan. It was important that sampling methods were uniform at each grain measurement location. To be consistent, a 10-m radius was measured out at each location, and the long (A) and intermediate (B) axes lengths of every clast within the radius were recorded. Afterwards, calculations were performed to determine the B axis value in the 50^{th} percentile (D50), 90^{th} percentile (D90) and 100^{th} percentile (Dmax) at each location. Next, these values were interpolated in ArcGIS using the inverse distance weighted tool, located in the 3D Analyst toolbar. This approach helped evaluate how the values of D50, D90, and Dmax changed across the surface of each fan.

Fan Area Delineation

Fan areas were delineated to calculate fan volumes, vegetated fan area (see later), and to clip rasters generated during grain size interpolation. Fan areas were delineated using a hill-shade relief model of the 2006 Yosemite Valley LiDAR data set as a guide. With the aid of imagery, the fan boundaries were digitized using the editor toolbar in ArcGIS. In addition, the fan area was estimated using the Field Calculator.

Vegetated Area Calculations

Vegetated surface area was calculated to describe the physical state of each fan. Vegetated areas were determined for each fan using Supervised Image Classification,

located in the Spatial Analyst toolbar in ArcGIS. A 1-m orthoimage of Yosemite Valley from 2014 was used during this process. With user input, the tool was able to determine which pixels in the orthoimage represented vegetation. The resultant raster was converted into a polygon shapefile and the percentage of vegetated fan area was calculated for each fan by dividing the vegetated area by total fan area.

Average Fan Slope Calculations

Average fan slope was used to describe the physical state of each fan. A slope map was created for each site from the 2006 LiDAR imagery using the 3D Analyst toolbar. Next, raster values were exported to Excel using the Extract Values to Table tool located in the Geostatistical Analyst toolbar. Afterwards, average slope was calculated using Excel for each fan.

Debris Flow Levee Metrics

After debris flow levees were grouped into pairs, individual flow volumes were calculated using ArcGIS. Debris flow volume calculations were used to compare the magnitude of ancient and historic flows. Also, flow volumes and cosmogenic dates at Indian Creek were used to estimate a recurrence interval of debris flow deposition. This process assumed that all material transported in a flow is deposited as levees and not in a lobate snout. Levee volume was calculated using the following equation:

$$V_l = A_l * l \tag{3}$$

where A_l is cross sectional area of a levee (m^2), and l is the length of a levee (m). To account for variations in area, levee cross sections were taken at five equal intervals and the cross sectional area was averaged over the length of each levee. The cross sectional

area was calculated using the formula for the area of a triangle. Individual flow volumes were calculated by adding the volume of paired levees together. The distance between debris flow levees and individual levee length measurements were also estimated using ArcGIS. These measurements aided in recognizing if a relationship exists between flow width and length. Width measurements were taken at five equal intervals and averaged along the length of a debris flow. In some instances, the beginning and end of two levees are dramatically offset; in these instances fewer width measurements were taken. Afterwards, flow width was plotted versus length and versus flow volume. Next, linear regression analyses were used to test the hypothesis that wider debris flows have greater lengths and volumes.

Fan Volume Measurements

Fan volume was calculated at each site to explore how lithology and watershed area produce debris flow fans of different sizes. In addition, fan volumes were used to calculate watershed erosion rates at each site. The volumes of the Eagle Creek and Indian Creek fans were estimated in ArcGIS using the Surface Volume tool, located in the 3D Analyst toolbar. This tool calculates the volume of a deposit above a flat plane, with a defined elevation. This approach assumes that the valley floor is a flat plane, at a right angle to the valley wall. The surface of each fan was taken from the Yosemite Valley LiDAR Digital Elevation Model (DEM). For simplicity, the elevation of the valley floor was set equal to the lowest elevation of each fan. A different methodology was used at Sentinel Creek because the fan is deposited against a talus slope instead of against the valley wall. At this location, fan volume was calculated by estimating the

volume of material between the fan surface and the talus pile. In this case, the volume was estimated using the Cut and Fill tool, located in the 3D Analyst tool bar, which estimates the volume between two surfaces. The talus surface was modeled under the fan as a flat plane with a constant slope using a spline interpolation method. In addition, this approach assumes that the valley floor is flat and that the talus slope and fan intersect the valley floor at the same elevation.

Erosion Rate Calculations

An erosion rate was calculated for each watershed to compare rates of erosion across all field sites. Erosion rates were calculated using the following equation:

$$E = (V_f/A_s) / t \quad (4)$$

where V_f is the volume (m^3) of the fan, A_s is the source area (m^2), and t is the age of the glacial retreat. Erosion rates were calculated using an age of 19.8 ky, which is the average depositional age of the terminal moraine found in El Capitan Meadow (Stock and Uhrhammer, 2010). This age is representative of the time when final glacial retreat began. The fans must postdate glacial recession, because the glacier cleared the valley of earlier deposits before its recession. The erosion rate was calculated in units of millimeters per year (mm/y).

In order to calculate a minimum and maximum erosion rate, both watershed and a rock source areas needed to be delineated for each field site. These source areas were used because they describe two specific places where fan sediments originate. A rock source area was delineated by determining where slopes exceeded 32° along each watershed. At this angle, any loose talus would maintain motion and fall into the

channels along Indian Creek and Eagle Creek, or onto the talus pile at Sentinel Creek. At Indian Creek and Eagle Creek, a maximum erosion rate was calculated using the rock source area, while a minimum rate was calculated using the entire watershed area. Erosion rates are greater along the rock source areas, because this area is smaller when compared to the entire watershed. Because of the unique geometry of the Sentinel Creek fan, three erosion rates were calculated at this site. The first rate measured sediment transfer from the rock source area to the talus pile (Fig. 5A). A second rate estimated sediment transfer from the rock source area to both the talus pile and fan (Fig. 5B). Last, a third rate calculated sediment transfer from the talus pile to the fan (Fig. 5C).

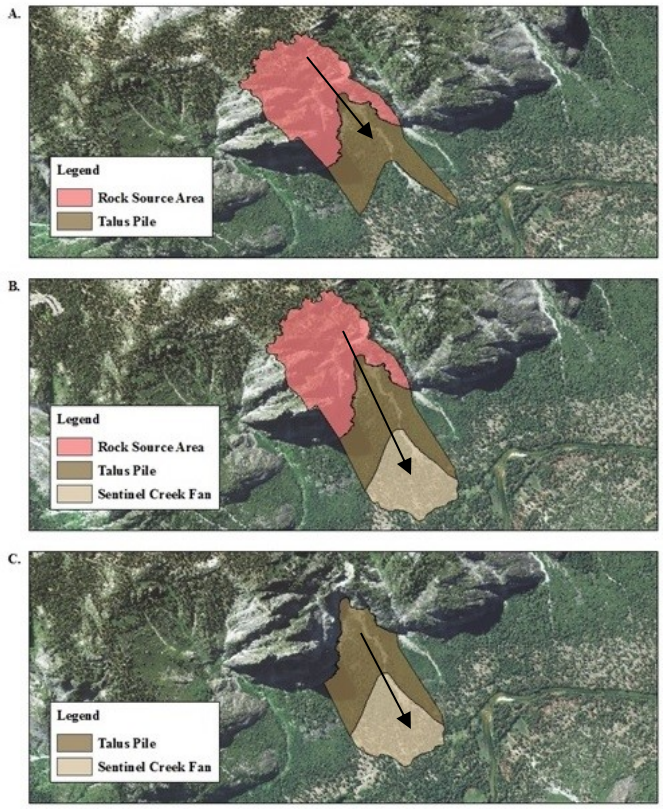

Figure 5A. Arrow indicates the movement of sediment from the Sentinel Creek rock source area to the talus pile. Figure 5B. Arrow indicates the movement of sediment from the rock source area to the talus pile and fan combined. Figure 5C. Arrow indicates the movement of sediment from the talus pile to the fan.

RESULTS

Indian Creek Fan

The Indian Creek fan has an area of 2.10×10^5 m^2, an average slope of 12°, and is approximately 72 percent vegetated (Table 1).

TABLE 1. FAN AREA, PERCENT VEGETATION, AND AVERAGE FAN SLOPE

Field Site	Total Fan Area (m^2)	Vegetated Area (m^2)	Percent Vegetation (%)	Slope (°)
Indian Creek	210,008	150,471	72	12.2
Eagle Creek	281,141	205,621	73	11.8
Sentinel Creek	178,266	113,079	63	11.7

The active channel is currently loaded with debris. A total of seven levees were mapped on the Indian Creek fan; these levees are located along the western edge of the fan and trend to the southeast (Fig. 6). Six of the debris flow levees were paired together, leaving one unmatched levee. Levees begin near the apex of the fan and extend toward the mid reaches of the fan. Cross-cutting relationships demonstrate that levees become progressively older to the west. The paired debris flow levees on the Indian Creek fan have an average volume of 21,979 m^3 (Appendix A1). The distances between paired levees range from 10 to 19 m, while levee lengths range from 91 to 556 m (Appendix B1). The widths between debris flow levees increase with flow length and flow volume (Figs.7 and 8). Grain size measurements were taken at fourteen locations on the fan. The values of D50, D90, and Dmax averaged 0.68 m, 1.34 m, and 2.29 m, respectively (Appendix C1). Values of D50, D90, and Dmax were greater at the apex of the fan than at the toe of the fan (Figs. 9, 10 and 11).

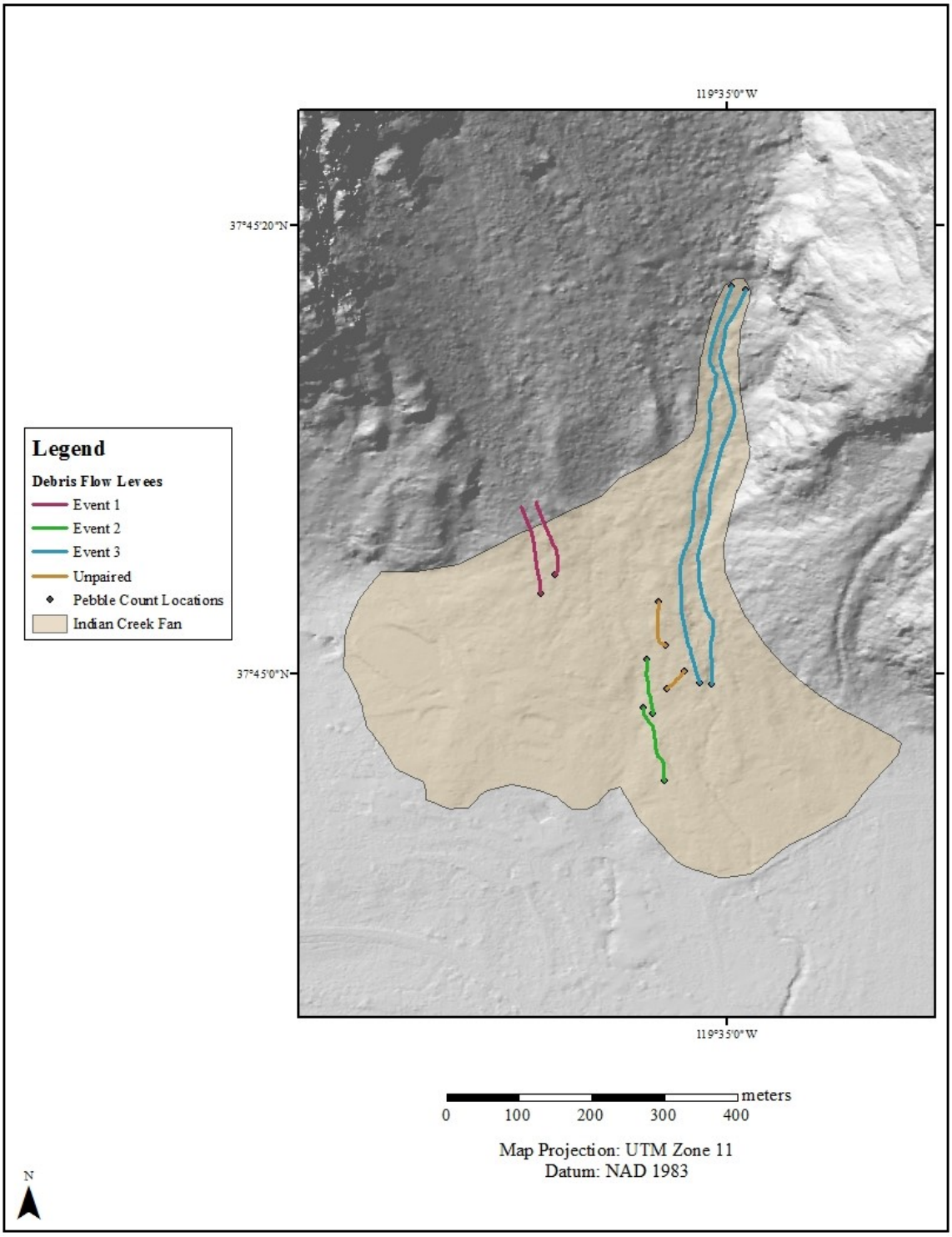

Figure 6. Map of debris flow levees on the surface of the Indian Creek fan.

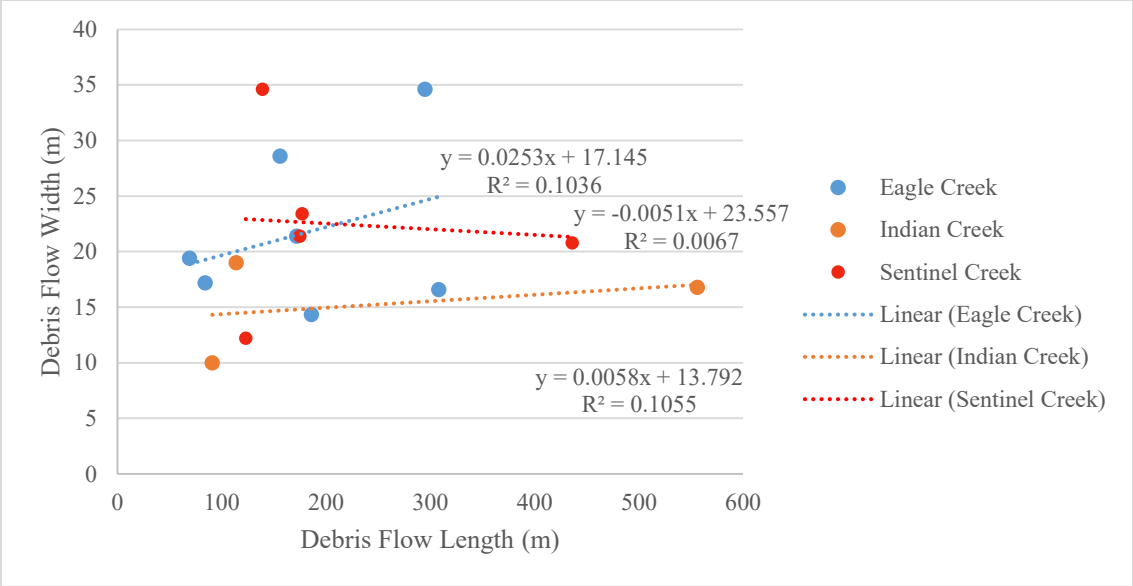

Figure 7. Plot comparing the widths between debris flow levees and levee lengths for the Indian Creek, Eagle Creek, and Sentinel Creek fans.

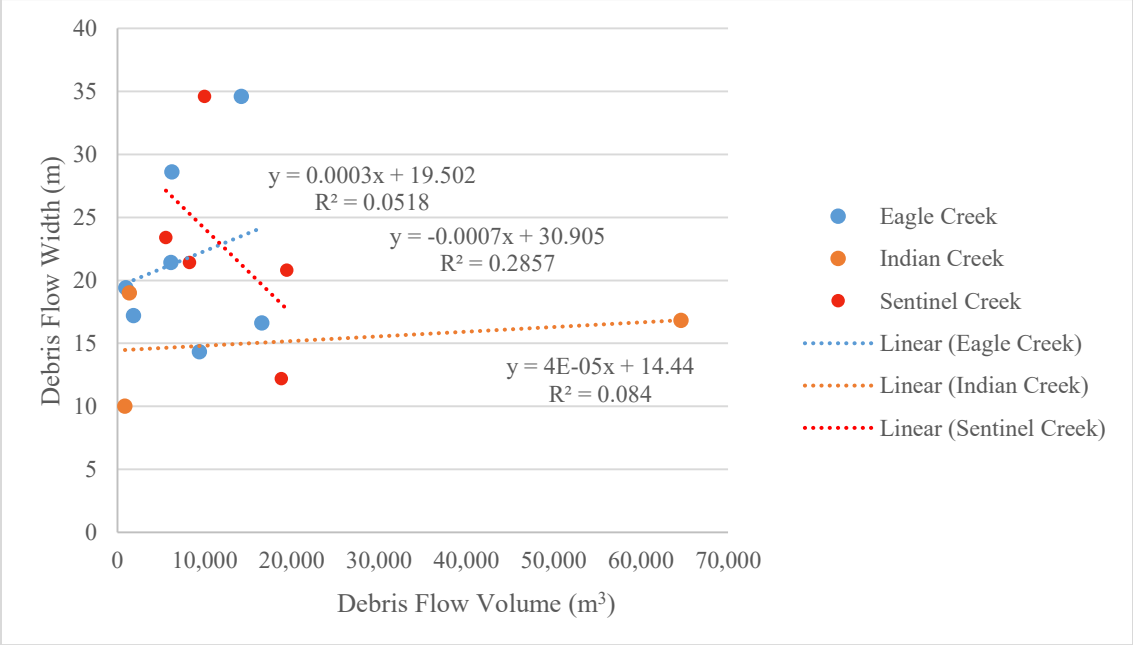

Figure 8. Plot comparing the widths between debris flow levees and paired levee volumes for the Indian Creek, Eagle Creek, and Sentinel Creek fans.

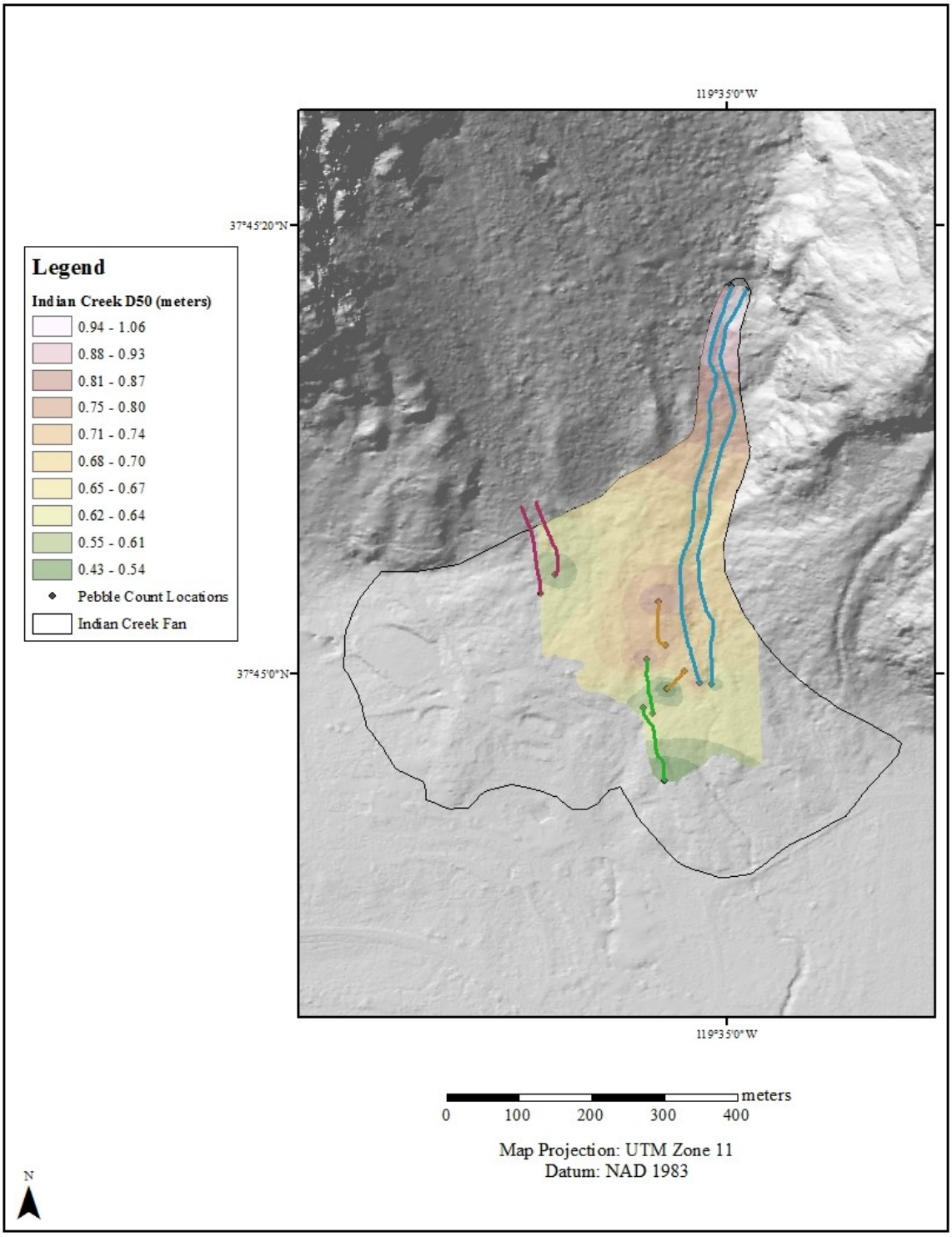

Figure 9. Map of the spatial distribution of D50 values on the surface of the Indian Creek fan.

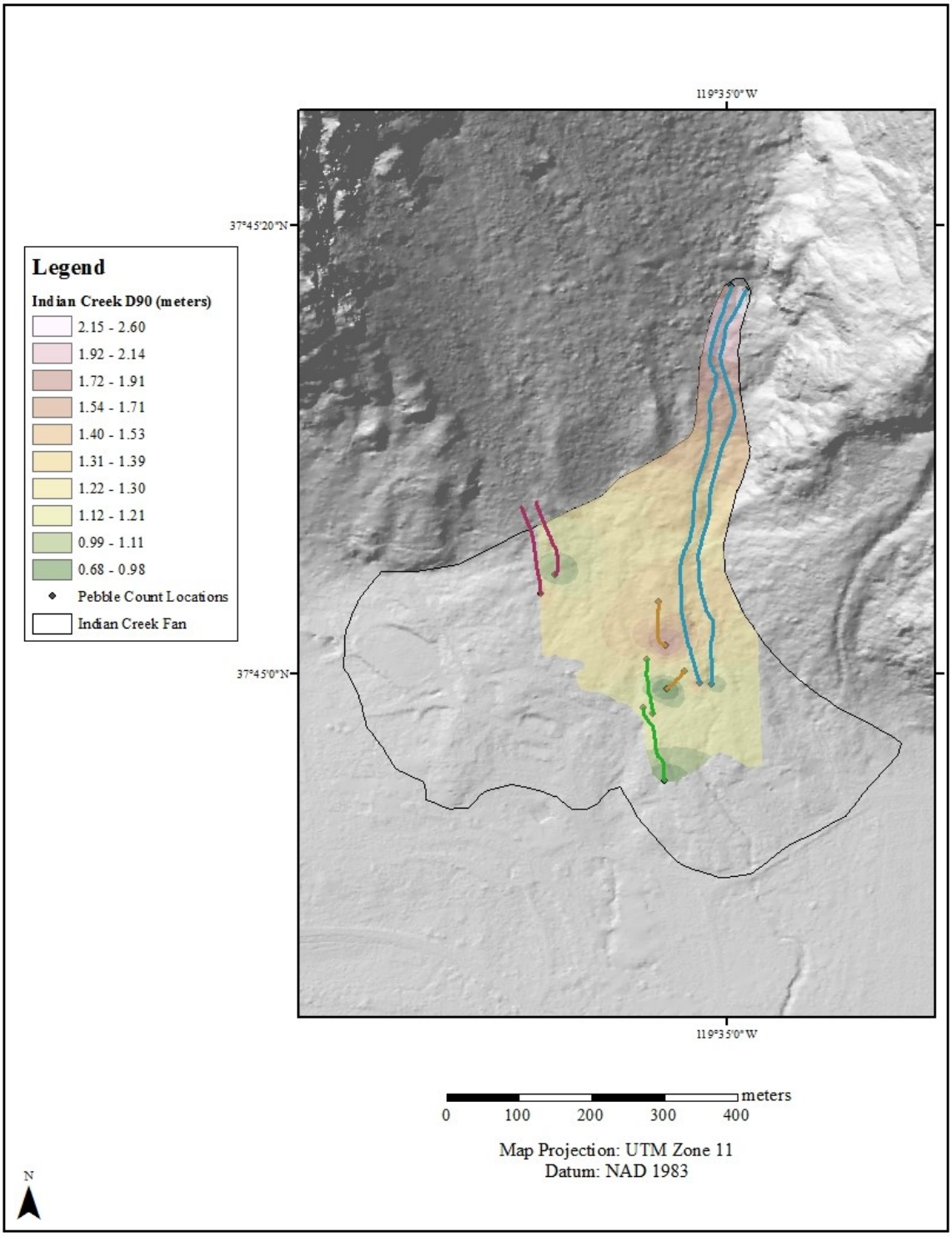

Figure 10. Map of the spatial distribution of D90 values on the surface of the Indian Creek fan.

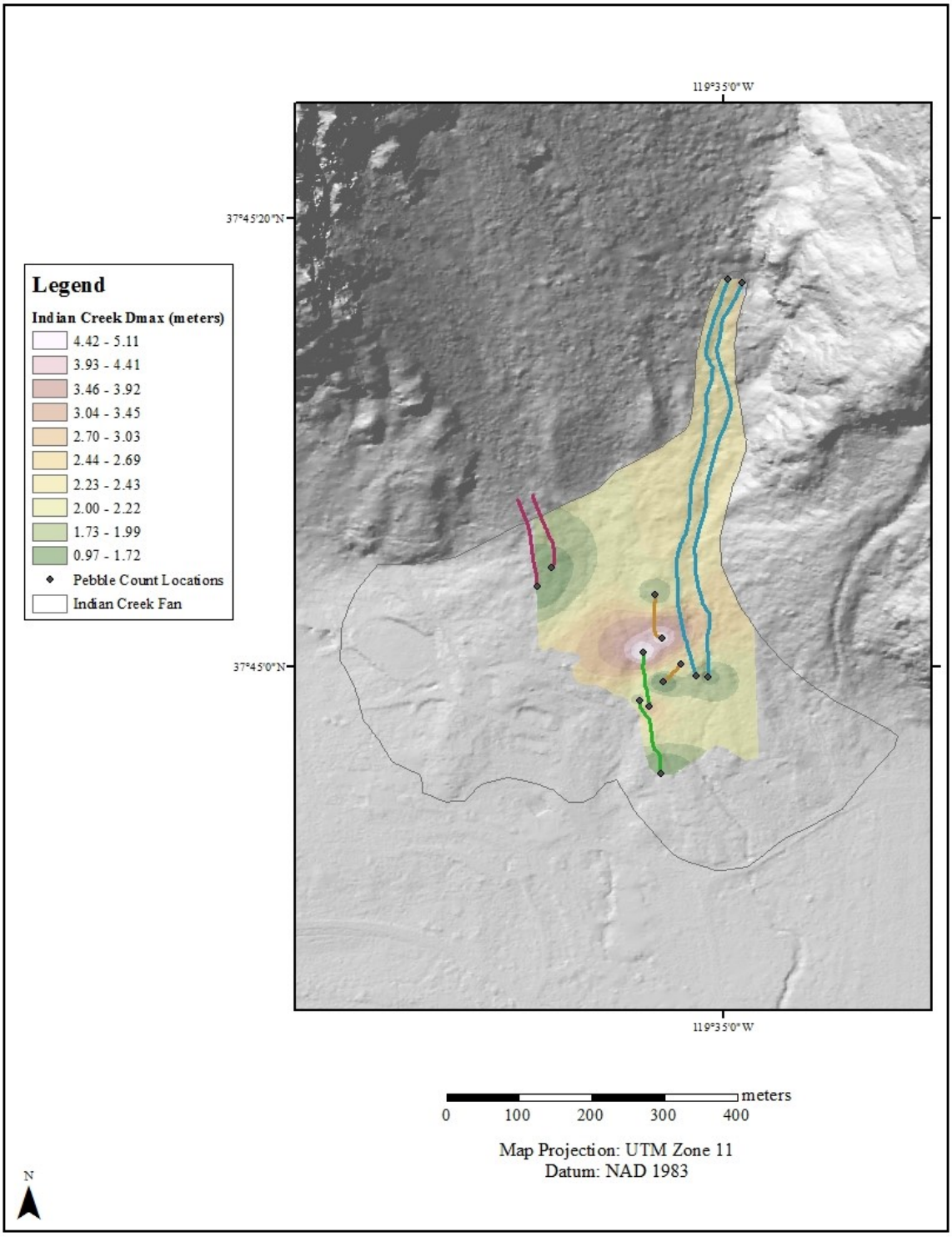

Figure 11. Map of the spatial distribution of Dmax values on the surface of the Indian Creek fan.

^{10}Be exposure dating indicated that the youngest levees were deposited on the Indian Creek fan between 9.6 ka-14.5 ka years ago, with an average depositional age of 12.1 ka (Fig. 12, Table 2).

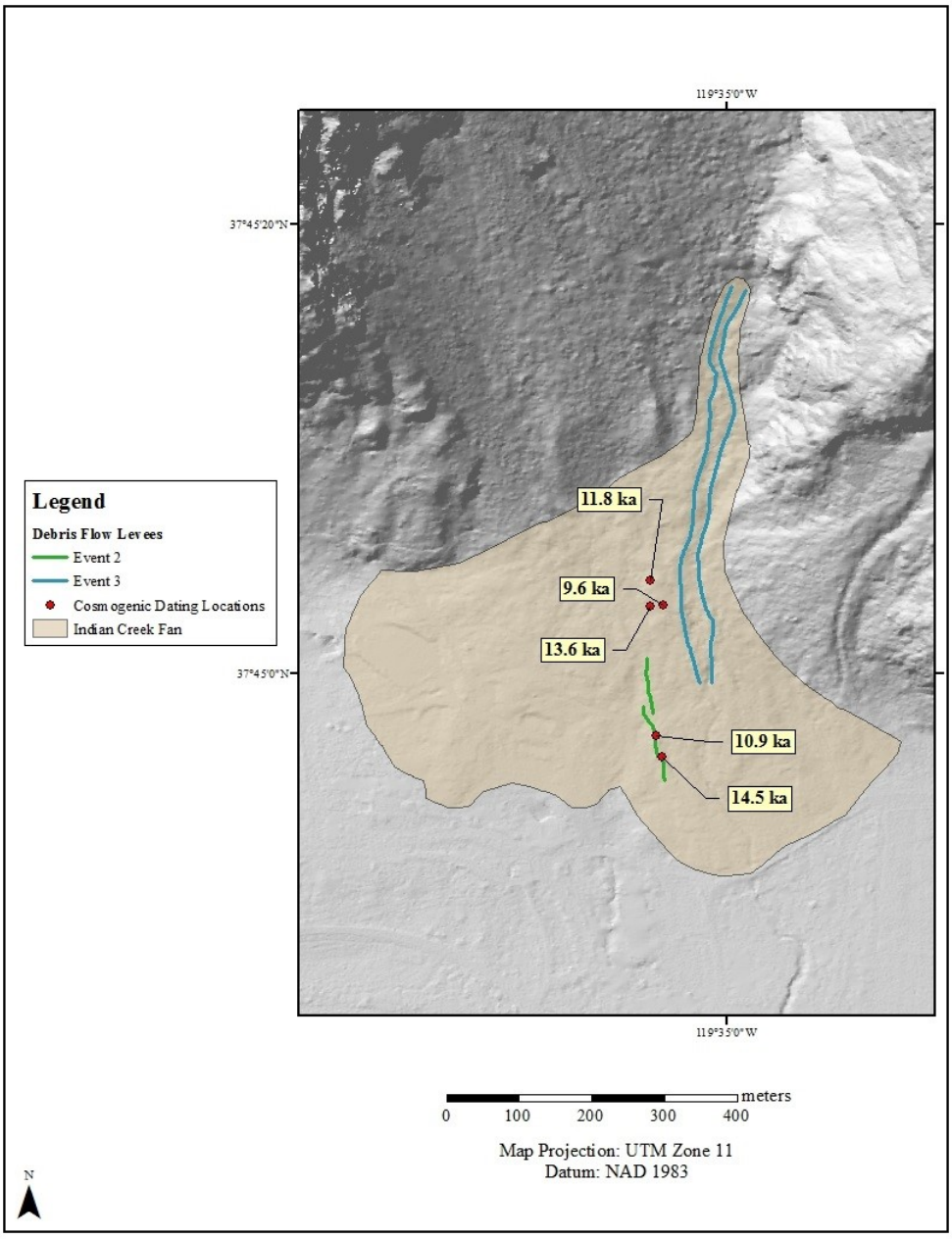

Figure 12**.** Map of the ^{10}Be cosmogenic samples locations and corresponding ages. Samples on event 2 were collected from the crest of the levee. Sample locations are offset on event 2 because levees were mapped from the inside of the channel.

TABLE 2. COSMOGENIC EXPOSURE AGES ON THE INDIAN CREEK FAN

Sample Name	Sample Location		Elevation	Be-10 Exposure Age
	Latitude (DD)	Longitude (DD)	(m)	(y)
IC-DF1-1	37.75110	119.58428	1,311	11,758
IC-DF1-2	37.75079	119.58428	1,293	13,563
IC-DF1-3	37.75080	119.58412	1,280	9,658
IC-DF2-1	37.74917	119.58420	1,240	10,937
IC-DF2-2	37.74891	119.58414	1,241	14,514

Maximum and minimum erosion rates for Indian Creek were between 0.55 mm/y - 0.07 mm/y (Table 3).

TABLE 3. EROSION RATE CALCULATIONS AT INDIAN, EAGLE, AND SENTINEL CREEKS

Field Site	Deposite Volume (m^3)	Source Surface Area (m^2)	Age (y)	Erosion Rate (mm/y)
Indian Creek				
Maximum	6,226,234	1,475,122	7,700	0.55
Minimum	6,226,234	11,718,842	7,700	0.07
Eagle Creek				
Maximum	7,452,419	1,752,807	19,800	0.21
Minimum	7,452,419	3,789,318	19,800	0.10
Sentinel Creek				
Rock Source Area to Talus Pile	36,228,091	899,873	19,800	2.03
Rock Source Area to Talus Pile and Fan	41,553,726	899,873	19,800	2.33
Talus Pile to Fan	2,130,035	81,760	19,800	1.32

Eagle Creek Fan

The Eagle Creek fan has an area of 2.81×10^5 m^2, an average slope of 12°, and is approximately 73 percent vegetated (Table 1). The upper reaches of the active channel are currently loaded with debris. A total of seventeen levees were mapped on the Eagle Creek fan. Fourteen of the levees were paired together, leaving three unmatched levees. Debris flow levees occupy the entire fan surface. The levees radiate from just below the fan apex and extend to below the middle of the fan. Cross-cutting relationships on the fan surface show that levees become progressively older to the west (Fig. 13).

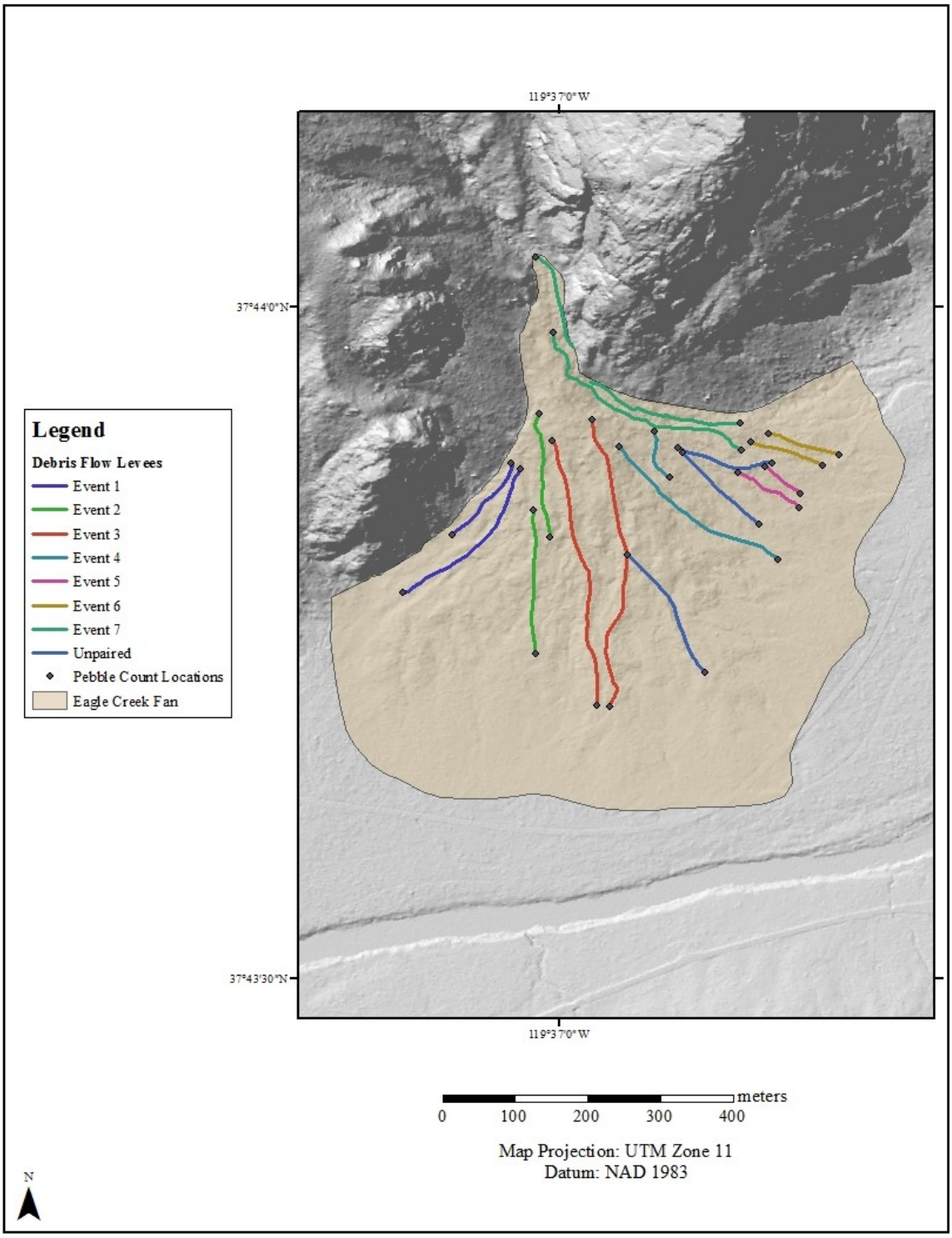

Figure 13. Map of debris flow levees on the surface of the Eagle Creek fan.

The paired debris flow levees on the Eagle Creek fan have an average volume of 7903 m^3 (Appendix A2). The distances between paired levees range from 14 to 35 m, while levee lengths range from 69 to 308 m (Appendix B2). The widths between debris flow levees increase with flow length and volume (Figs. 7 and 8). Grain size measurements were performed at thirty-four locations on the fan surface. The value of D50, D90, and Dmax averaged 0.68 m, 1.34 m, and 1.89 m, respectively (Appendix C2). Values of D50, D90, and Dmax were higher at the apex of the fan than at the toe of the fan (Figs. 14, 15 and 16). No cosmogenic dating was performed at this site; therefore, a depositional age of 19.8 ka was used. Maximum and minimum erosion rates for Eagle Creek were between 0.21 mm/y - 0.10 mm/y (Table 3).

Sentinel Creek Fan

The Sentinel Creek fan has an area of $1.78x10^5$ m^2, an average slope of 12°, and is approximately 63 percent vegetated (Table 1). A total of twenty levees were mapped on the Sentinel Creek fan, of which ten were mapped in the field and ten were mapped from the LiDAR DEM. Ten debris flows were paired together, leaving ten unmatched levees. Two groups of debris flow levees were found; one group begins at the fan apex and terminates mid-fan, and the second, older group begins below the first group and extends to the toe of the fan. Levees trend to the northwest and occupy the western portion of the fan. Cross-cutting relationships reveal that levees become progressively older to the east (Fig. 17). The paired debris flow levees along Sentinel Creek have an average volume of 10,334 m^3 (Appendix A3). The distances between paired levees range from 12 to 35 m, while levee lengths range from 123 to 436 m (Appendix B3).

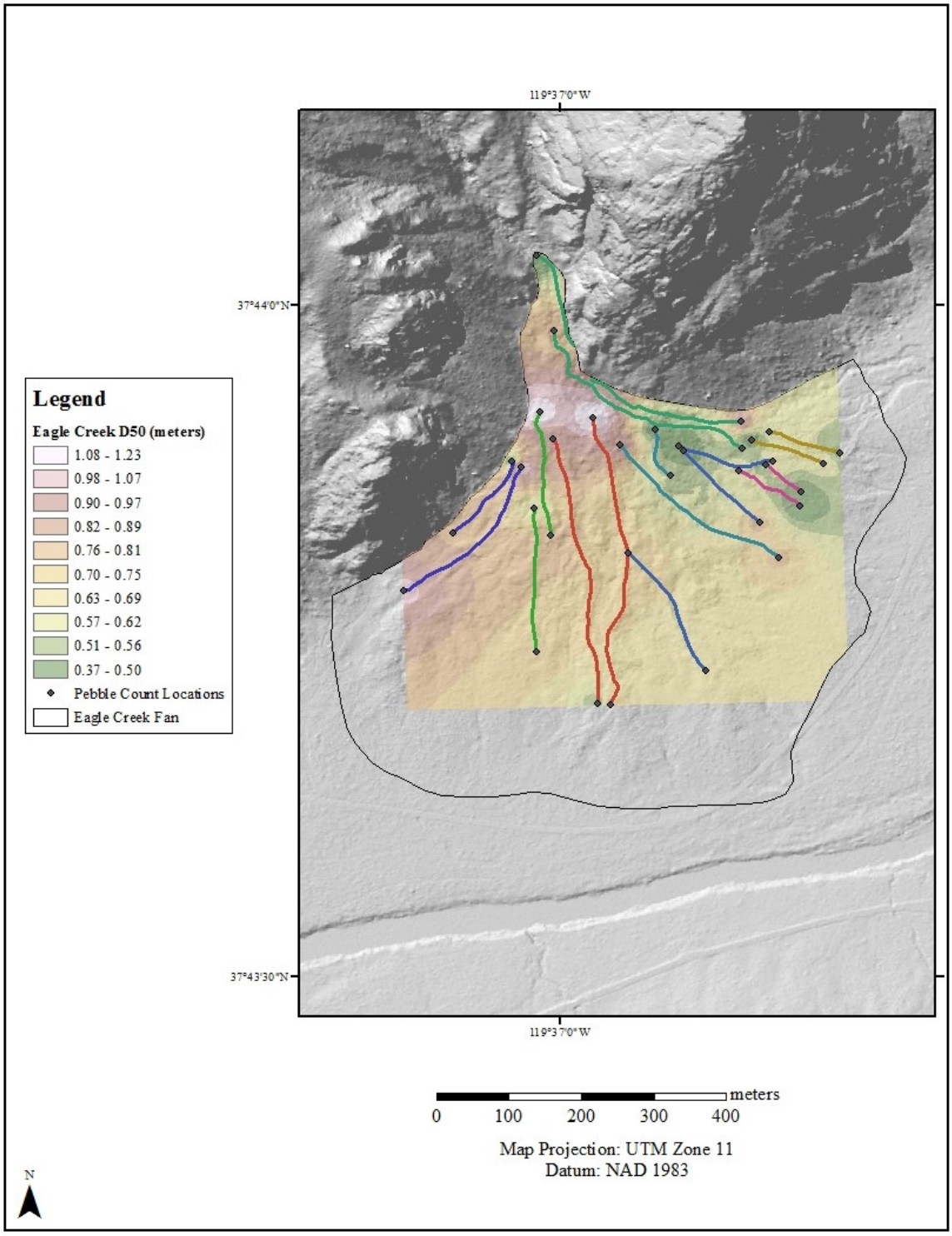

Figure 14. Map of the spatial distribution of D50 values on the surface of the Eagle Creek fan.

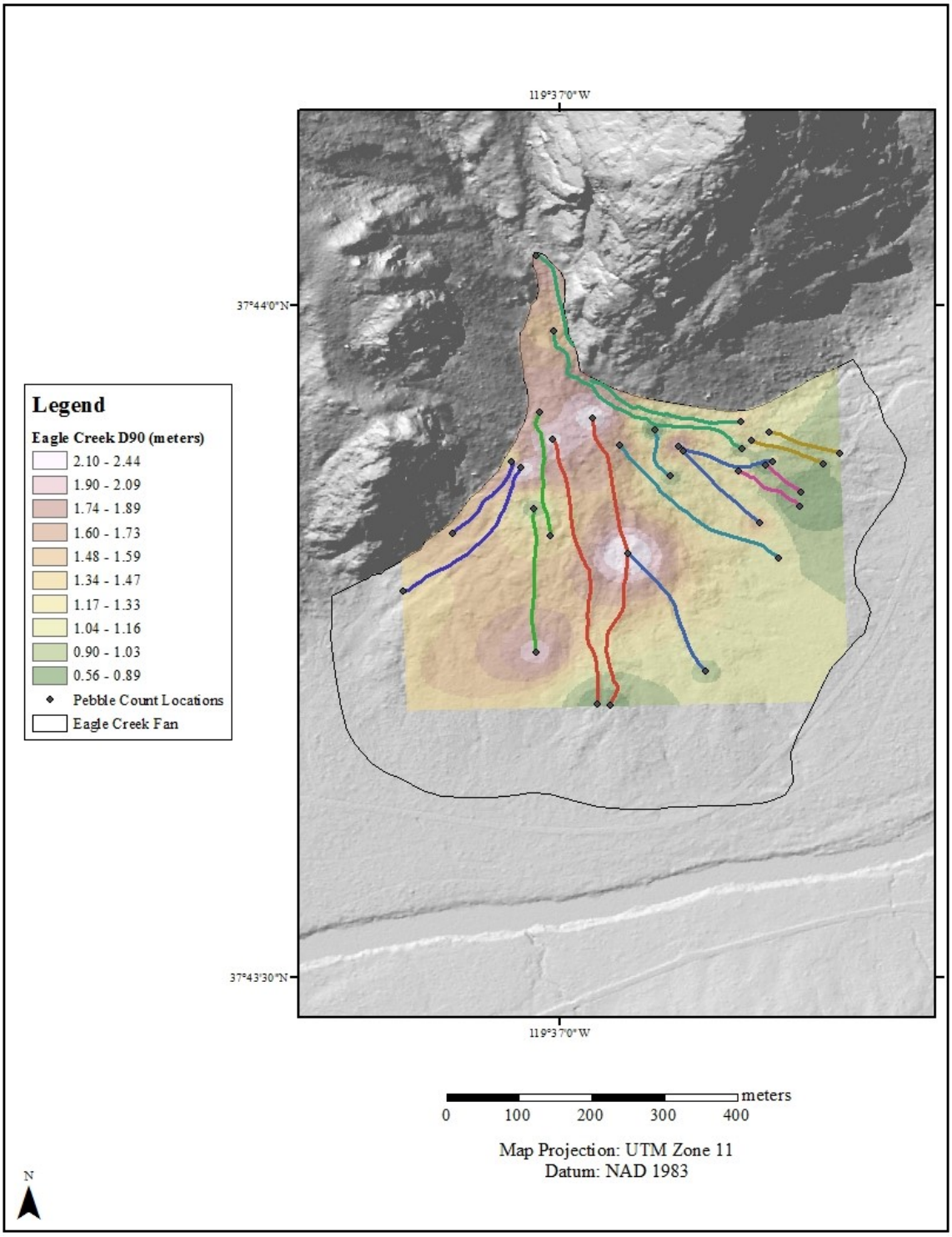

Figure 15. Map of the spatial distribution of D90 values on the surface of the Eagle Creek fan.

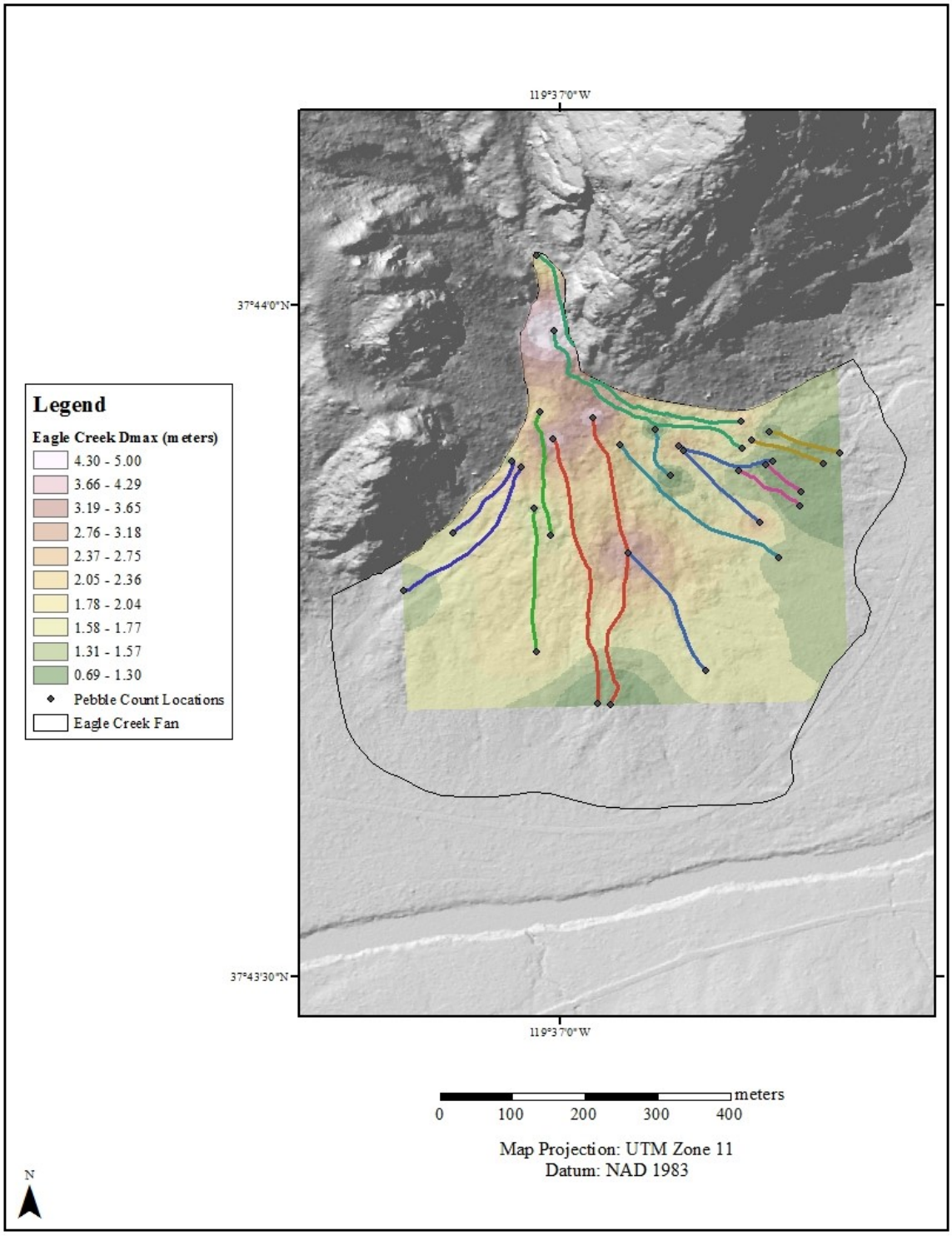

Figure 16. Map of the spatial distribution of Dmax values on the surface of the Eagle Creek fan.

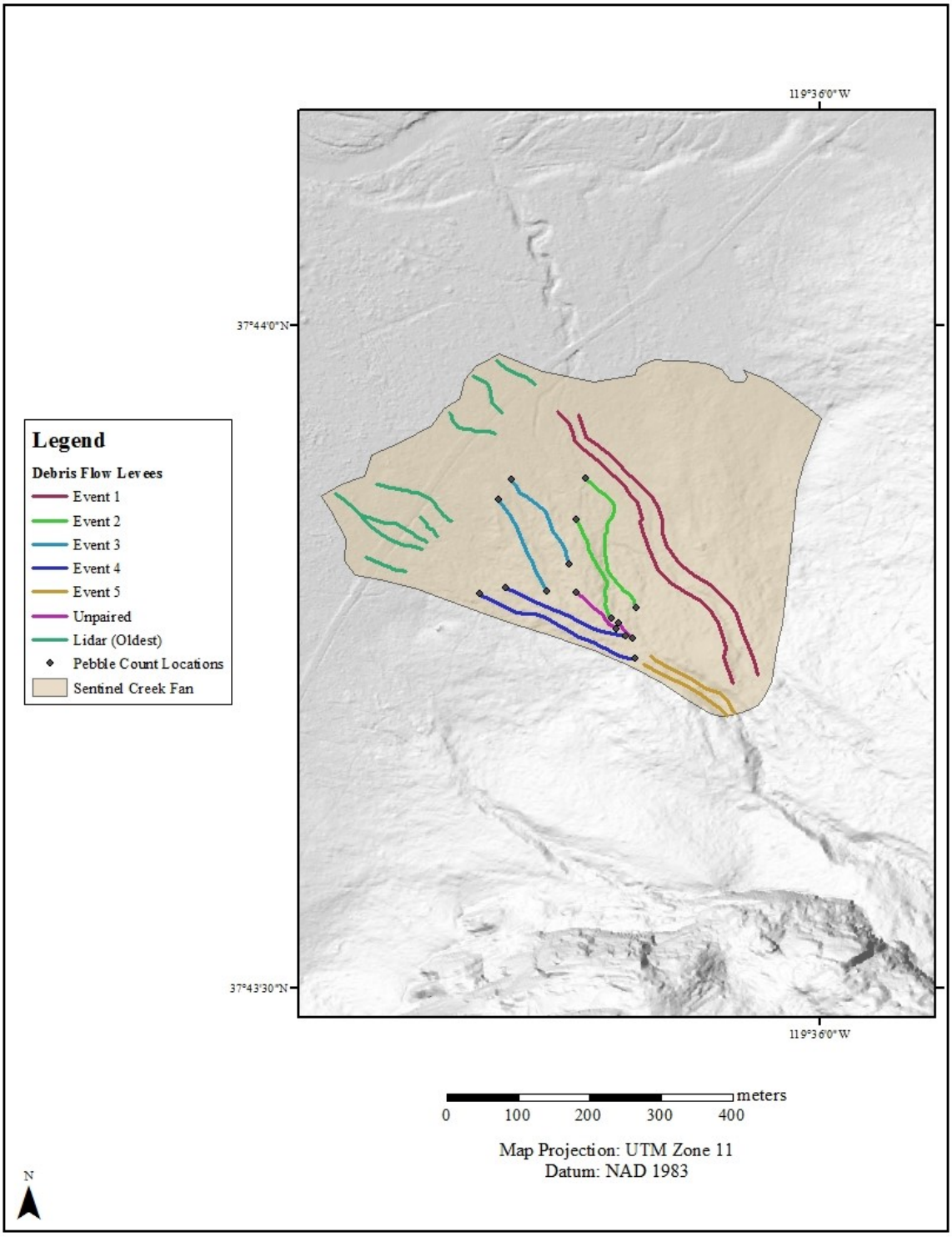

Figure 17. Map of debris flow levees on the surface of the Sentinel Creek fan.

The widths between debris flow levees decrease with flow length and volume (Figs. 7 and 8). Grain size measurements were performed at sixteen locations. The value of D50, D90, and Dmax averaged 0.41 m, 0.87 m, and 1.35 m, respectively (Appendix C3). Values of D50, D90, and Dmax were higher at the apex than the toe of the fan (Figs. 18, 19 and 20). No cosmogenic dating was performed at this site; therefore, a depositional age of 19.8 ka was used for calculating the three erosion rates for Sentinel Creek. A rate of 2.03 mm/y was calculated for the transfer of sediment between the rock source area and talus pile. A second rate of 2.33 mm/y was estimated for the transfer of sediment from the rock source area to the talus pile and debris fan combined. Last, a rate of 1.32 mm/y was estimated for sediment transfer between the talus pile and debris fan (Table 3).

DISCUSSION

Sediment Size Distribution

Average values of D50, D90, and Dmax measured along the Eagle Creek and Indian Creek fans are almost identical to each other. In contrast, the average values of D50, D90, and Dmax along Sentinel Creek are up to two times smaller than those of Eagle Creek and Indian Creek (Appendix C). Even though differences in clast sizes exist between the three fans, it is still plausible that a similar process generated debris flow material at all three sites. Slope failure, caused by glacial debuttressing and weathering, provided catchments in Yosemite Valley, with more available sediment after the LGM when compared to the interglacial period. Evans and Clague (1994) demonstrated that glacial debuttressing causes fractures and joints through glacial valleys, which ultimately leads to the failure of steep bedrock surfaces.

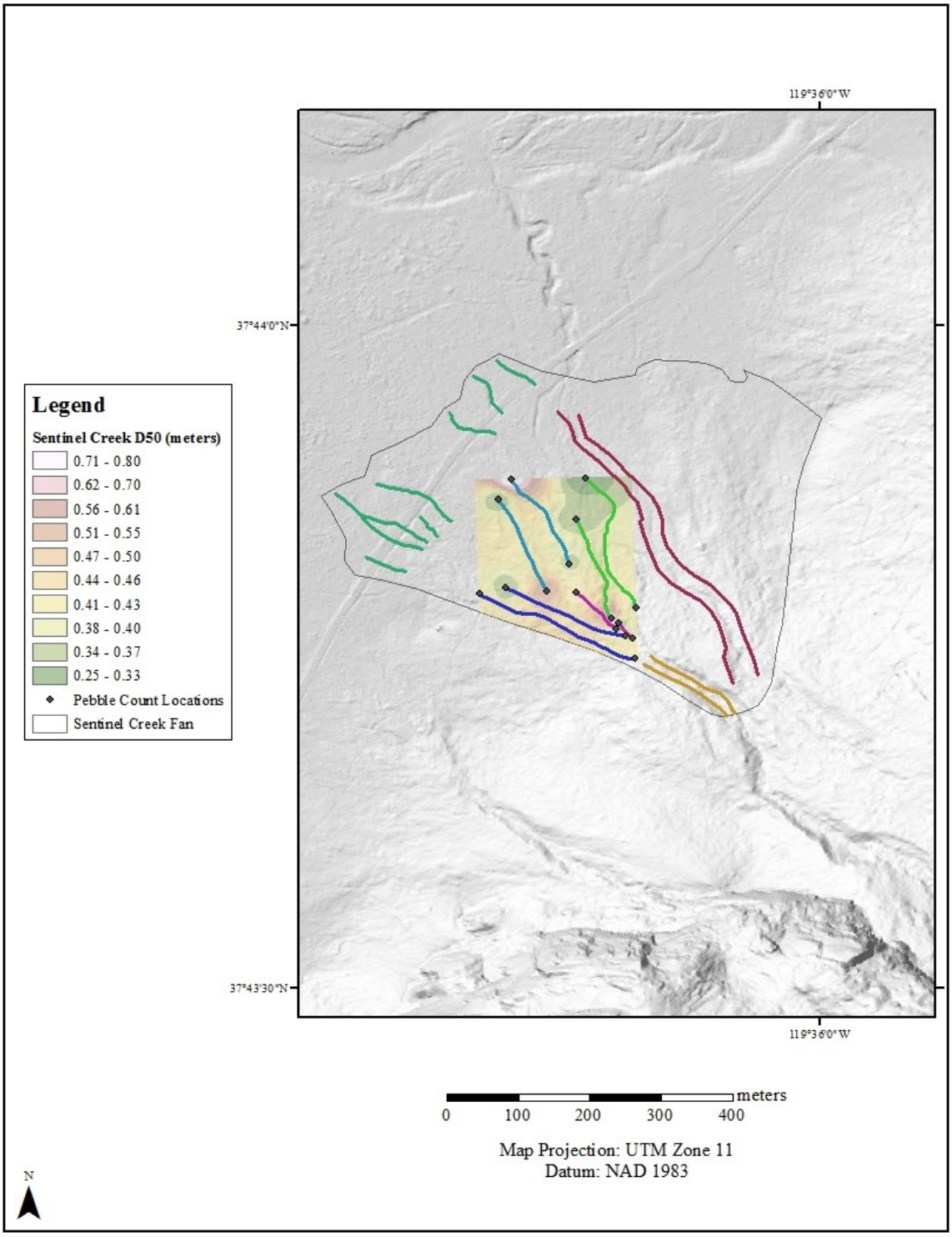

Figure 18. Map of the spatial distribution of D50 values on the surface of the Sentinel Creek fan.

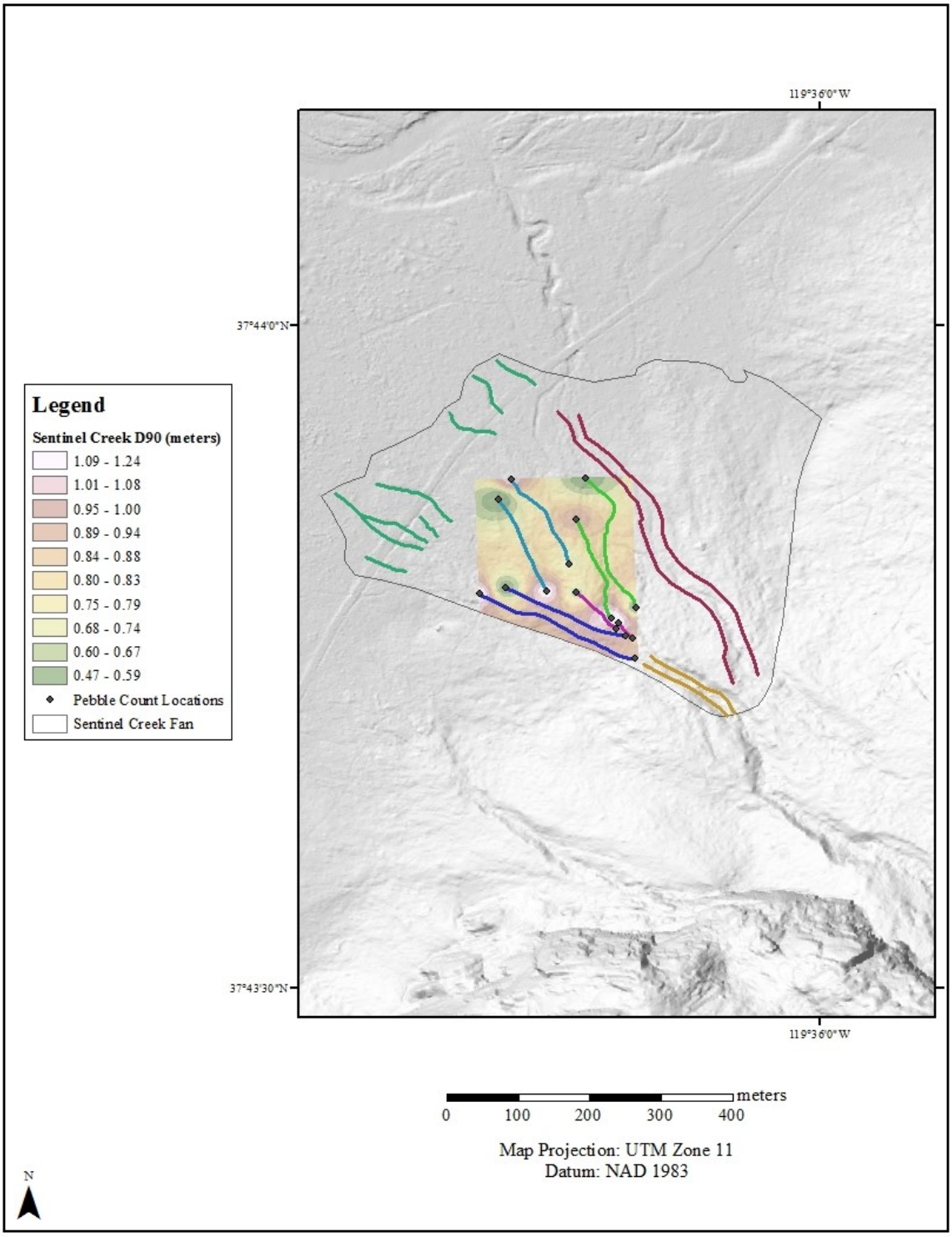

Figure 19. Map of the spatial distribution of D90 values on the surface of the Sentinel Creek fan.

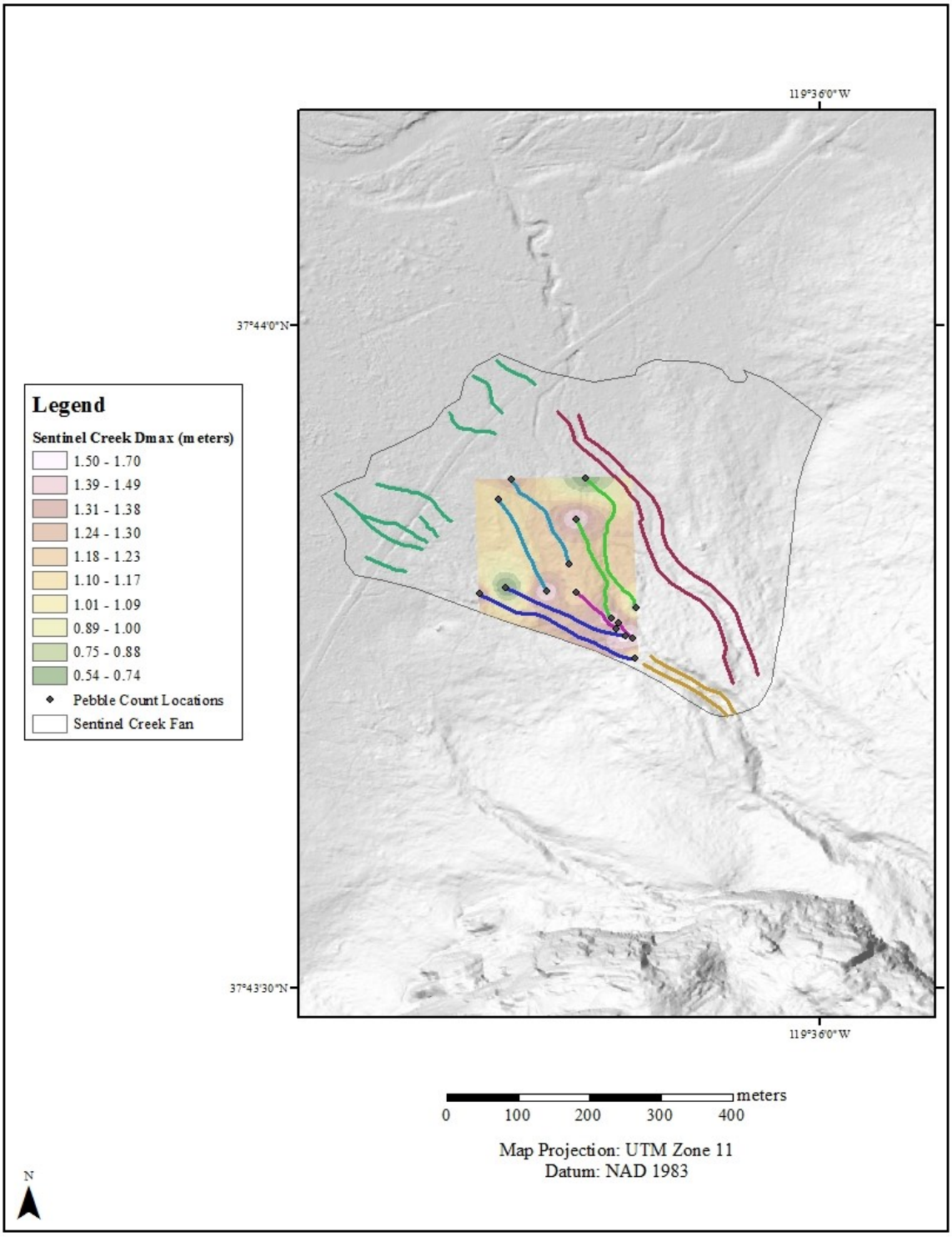

Figure 20. Map of the spatial distribution of Dmax values on the surface of the Sentinel Creek fan.

Previous studies of other glaciated valleys have used cosmogenic dating to demonstrate that slope failures are frequent during glacial debuttressing (Cossart et al., 2008), while others note that bedrock failure postdates glaciation by hundreds to thousands of years (Ballantyne and Stone, 2004; Stock and Uhrhammer, 2010). The Eagle Creek and Indian Creek fans are below steep, ephemeral channels that flow between large cliffs and the Sentinel Creek fan is below a large cliff face and waterfall. Due to the proximity of large cliffs to the three field sites, it is likely that slope failure loads channels with debris and then the channels are cleared out by high discharges. However, the majority of rock fall in Yosemite Valley has occurred above the Tioga trim line. Rock fall is more prominent in these areas because they have been weathered over a longer period of time (Brody et al., 2015). It is hypothesized that slope failure caused by glacial debuttressing and weathering produced the loose sediment in each watershed.

During GIS analysis, a spatial relationship between clast size and clast position on the fan was found. At all sites, boulders become progressively smaller from the apex toward the toe of the fan. The deposition of larger grains closer to the apex plays an important role in fan growth as it pertains to debris flow deposition. During debris flow deposition, grain segregation causes sediment sorting in levees. Experimental debris flow observations show that larger material is transported through the flow head and deposited as levees first (Johnson et al., 2012). As the flow continues downhill, progressively smaller material is deposited onto each levee. As the debris flow loses momentum, any remaining material is deposited as a lobate snout (Johnson et al., 2012).

Sediment sorting during debris flow deposition may control the spatial distribution of debris flow sediments at each field site.

Debris Flow Metrics

At each site, the distances between debris flow levees were plotted against flow lengths and flow volumes. This method was used to test the hypothesis that wider debris flows have greater lengths and volumes. At Indian Creek and Eagle Creek, there is a slight positive relationship between levees distances and flow lengths and also the relationship between levee distances and flow volumes (Figs. 7 and 8). In contrast, at Sentinel Creek a negative relationship was found, when using the same parameters. The results suggest that the distances between flow levees are not dependent on flow volumes or flow lengths. Additionally, the distances between the debris flow levees could be controlled by fan surface accommodation space. As debris flows spread across a fan, there is less room for subsequent flows across its surface.

Fan Volume Estimates

The results of fan volume estimates indicate that fan volume varies between each of the field sites. The volume of the Eagle Creek and Indian Creek fans are approximately three times the size of the Sentinel Creek fan. The differences in fan volume may be related to differences in watershed area, rock source area, and bedrock lithology. It is apparent that fan volume increases with larger watershed and rock source areas. It is likely that large source areas produce bigger fans because more sediment accumulates in these areas. Debris flows are able to capture and transport more material in a larger source area. Additionally, watershed lithology plays a minor role in fan

volume. The Eagle Creek watershed is composed of granite, while the Indian Creek and Sentinel Creek watersheds are composed of granodiorite (Calkins, 1985). Other studies have documented that granite landscapes are more resistant to weathering than granodiorite landscapes (Pye, 1986; Migoń and Vieira, 2014). If this relationship is true, the Indian and Sentinel Creek fans should have greater fan volumes than the Eagle Creek fan because their watersheds are composed of weaker material.

It is important to consider the different sources of error introduced by the methodologies used to estimate fan volume. The study modeled the valley floor as a flat surface beneath each fan. This approach does not account for any variation and relief in the valley floor. If the valley floor slopes downward, toward the valley wall, the study would underestimate fan volume. At Sentinel Creek, the fan is deposited below a talus pile. The study modeled the talus pile as a smooth surface with a constant slope that intersects the valley floor at the same elevation as the fan. Similarly, this approach does not account for any variation of the surface of the talus pile. A recent study used geophysical imaging to model the subsurface of Yosemite Valley and demonstrated that the valley wall meets the valley floor at an oblique angle (Brody et al., 2015). Consequently, the assumptions made during the estimations of fan volume were incorrect and fan volume was overestimated in the corner of the valley.

Erosion Rates

The average erosion rates of the Eagle Creek and Indian Creek watersheds are similar (Table 3). In contrast, the average erosion rate of the Sentinel Creek source area is up to ten times higher than that of Indian Creek and Eagle Creek (Table 3). Sediment

removal along Indian Creek and Eagle Creek is a supply-limited process. However, the Sentinel Creek fan sits below a large talus pile and, thus, has a continuous supply of material available for debris flow initiation. In contrast, the Indian Creek and Eagle Creek fans are below steep channels, where debris flows transport material that has fallen into the channel. At Eagle Creek and Indian Creek, a time lag must exist between the removal of material by a debris flow and the subsequent reloading of a channel by rock fall and dry ravel.

The Sentinel Creek fan is deposited below a talus pile, while the other two fans are not. Weaker bedrock lithologies may cause the formation of a talus pile, while bedrock jointing aids in channel development. Previous studies have suggested that the relief of granite landscapes is controlled by mineral texture (Migoń and Vieira, 2014) and composition (Pye, 1986). In general, fine-grained granitoids are stronger than medium- to coarse-grained varieties (Pye, 1986; Migoń and Vieira, 2014). Also, granitoids rich in potassium feldspar and quartz are stronger than varieties rich in biotite and pyroxene (Pye, 1986; Migoń and Vieira, 2014). These two relationships are supported by field observations where felsic and fine-grained granitoids are found in areas of higher elevation, while mafic and coarse-grained granites are found at lower elevations (Pye, 1986; Migoń and Vieira, 2014). The Sentinel Creek watershed is composed of Sentinel Granodiorite and the Indian Creek watershed is composed of Half Dome Granodiorite; both are rich in biotite and hornblende (Bateman, 1992). In contrast, the Eagle Creek watershed is composed of El Capitan Granite, which contains abundant potassium feldspar (Bateman, 1992). The studies mentioned above indicate that mafic bedrock is

weaker than felsic bedrock. The Sentinel Creek watershed may have a talus pile below it because the watershed is composed of weaker material. In comparison, the Indian Creek watershed is also composed of weaker material, but does not have a talus pile below it. For this reason, watershed lithology may be less important than once predicted. However, jointing could play a more important role in channel formation versus talus pile formation. Streams form preferentially along large master joints. These areas of highly fractured rock are easily eroded by fluvial and glacial processes (Ericson et al., 2005). Aerial views of Indian Creek and Eagle Creek show the presence of parallel joints along each channel. These joints extend from the rim of the valley to the valley floor (Figs. 21A and 21B). In comparison, at Sentinel Creek, jointing is less prominent along the valley wall, but is present on the valley rim (Fig. 21C). These observations suggest why a channel was never cut through the valley wall at the site of Sentinel Creek.

Timing of Debris Flow Deposition

The distribution of debris flow levees at each field site show that debris flow deposition was once an active fan-building process in Yosemite Valley. While this study has limited cosmogenic dates, it is important to reiterate that the Indian Creek fan has not experienced a debris flow since approximately 12.1 ka. The cosmogenic dating suggests that the majority of the Indian Creek fan was quickly constructed after the LGM (19.8 ka). Some aspects of the post-glacial environment must have been more favorable to initiate debris flows than at the present time. As discussed before, debris flow initiation is dependent on loose sediment and high water flows.

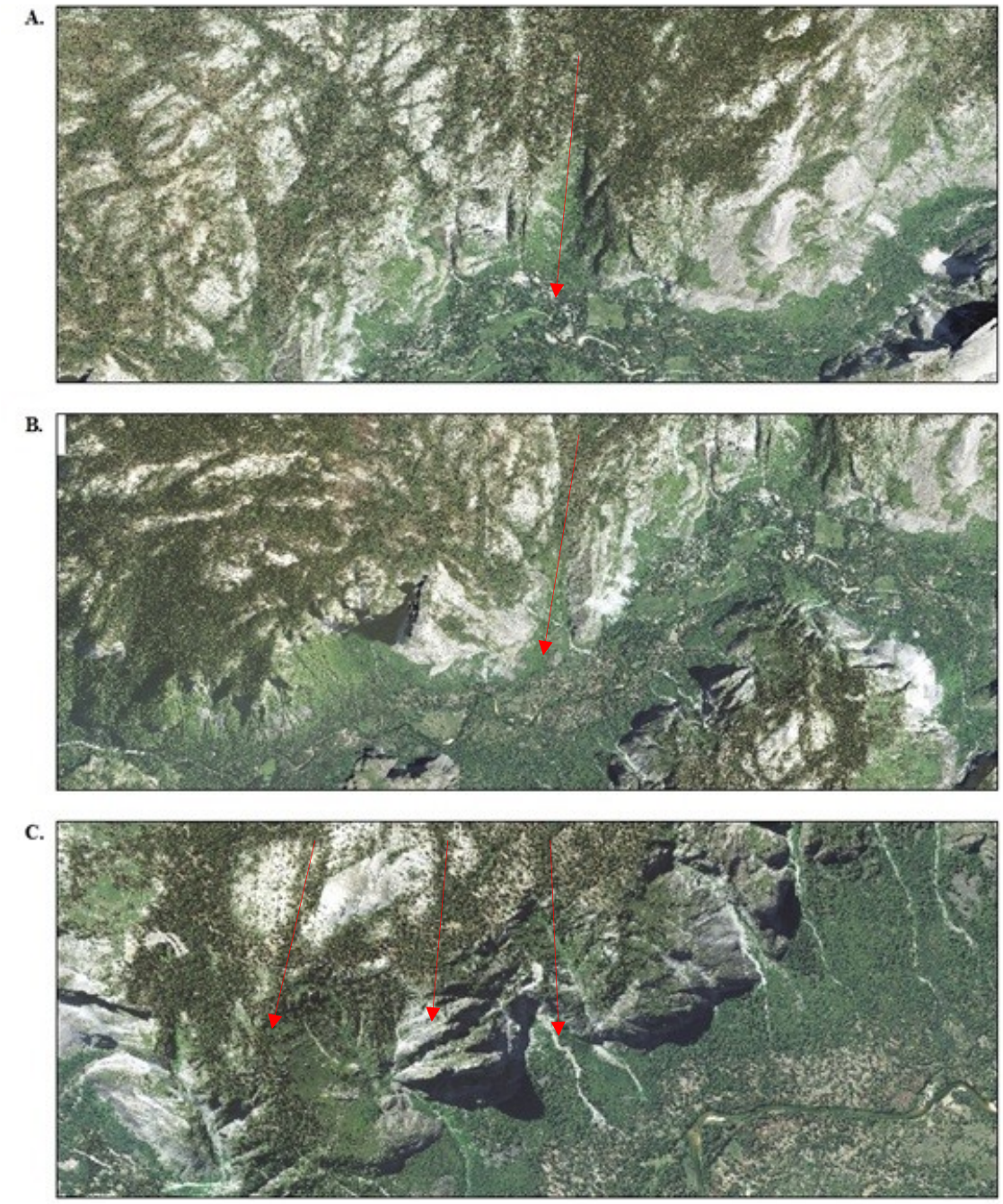

Figure 21A. The arrow indicates the position and orientation of sub-parallel jointing along Indian Creek. Figure 21B. The arrow indicates the position and orientation of sub-parallel jointing along Eagle Creek. Figure 21C. The arrows are pointing to lack of jointing along Sentinel Creek.

A wetter climate and an increase in sediment supply from glacial debuttressing during the end of the LGM was sufficient to produce numerous debris flows. In addition, discharge from rainfall during the present interglacial period has been too low to generate debris flows at the same frequency as during the LGM. Previous studies have used pollen and the abundances of carbon and nitrogen obtained from lake cores as proxies for paleo-climate (Smith and Anderson, 1992; Messing, 2001; Street et al., 2012). Pollen studies from Yosemite (Smith and Anderson, 1992) and Owens Valley (Messing, 2001) indicate that, in general, the Late Pleistocene was cooler and wetter than the Holocene. At these sites, high altitude species of mountain hemlock and juniper grew at lower elevations. The studies propose that both valleys were 4° to 5° C cooler during the Late Pleistocene (Smith and Anderson, 1992; Messing, 2001). Messing (2001) estimates that precipitation near Owens Valley was up to 80% higher than present. In addition, sediment cores at Swamp Lake in Yosemite National Park present a record of several low fluctuations in total organic carbon after the glacial period (Street et al., 2012). These conditions are indicative of a lake with a high input of sediment and water. Out of the three field sites in Yosemite Valley, this study confirms that the Indian Creek fan was quickly deposited after glaciation. The timing of deposition at Indian Creek could reflect a paraglacial exhaustion model (Church and Ryder, 1972; Ballantyne, 2002). Previous authors have suggested that sedimentation is higher following de-glaciation due to increased sediment supply and higher rates of runoff (Church and Ryder, 1972; Ballantyne, 2002). In addition, glacial debuttressing generates more sediment on hillslopes and in channels. Following de-glaciation, the rates of deposition in glaciated areas decrease asymptotically

toward pre-glacial levels. Rates of deposition decrease as the influx of paraglacial sediment exits a fluvial system (Church and Ryder, 1972; Ballantyne, 2002). Fluvial systems may take up to tens of thousands of years to reach pre-glacial sedimentation rates again (Ballantyne, 2002). Further cosmogenic dating at Eagle Creek and Sentinel Creek is needed to determine if the model is valid at all three of the field sites in Yosemite.

From 1857 to 2003, there were thirty-three historic debris flows documented in Yosemite Valley. These debris flows had an average volume of 1,029 m^3 (Wieczorek and Snyder, 2004). In contrast, the prehistoric debris flows mapped along Indian, Eagle, and Sentinel creeks have average estimated volumes of 22,771 m^3, 8,171 m^3, and 10,689 m^3, respectively. Different environmental factors must have produced prehistoric debris flows that are more than two times larger in magnitude than historic flows. The debris flows on the Indian, Eagle, and Sentinel Creek fans are predominately larger than the historic flows. The levees of small prehistoric debris flows, similar to the thirty-three documented events, could have faded and are no longer recognizable at each field site.

^{10}Be exposure dating, fan volume, and average debris flow volume were used to calculate a debris flow recurrence interval for the Indian Creek fan. ^{10}Be cosmogenic dating suggests that the Indian Creek fan was active between 19.8 ka and 12.1 ka. An age of 7.7 ka was used to calculate a debris flow recurrence interval of 27 years for the Indian Creek fan. The calculated interval seems to be lower than expected. Differences in the recurrence interval is likely related to fan volume because the age of the fan is known. A larger fan volume would produce a shorter recurrence interval because more flows of equal volume would be needed to construct a larger fan. Furthermore, in

calculating the fan volume, it was assumed that the valley floor met the valley wall at a right angle. In contrast, researchers have used geophysical techniques that model Yosemite Valley as a curved surface (Brody et al., 2015). If this is the case, then fan volume was overestimated in the corner of the valley.

Debris Flow Fan Growth Model

Beaty (1963) and Hooke (1967) were the first authors to conceptualize debris flow fan construction. These studies noted that an active debris flow channel changes position on the surface of a fan through time. It was hypothesized that large boulder dams that formed during a debris flow event caused channel shifts. The damming effect causes subsequent flows to be diverted laterally, which changes the course of the active channel. This mechanism causes all parts of the fan to be traversed, which builds up the fan through a series of superimposed debris flow deposits (Beaty, 1963; Hooke, 1967; Beaty, 1970). In addition, it is not necessary for boulders to back-fill the entire length of an active channel to cause channel abandonment (Beaty, 1963, 1970). In contrast, researchers who study fluvial fans attribute channel shifts to back-filling, which raises the fan surface along the entire channel, causing the channel to be diverted laterally toward a lower part of a fan (Bull, 1964; Denny 1967; Bull, 1977; Hooke and Rohrer, 1979). The process of channel diversion was observed by Suwa and Okuda (1983), who studied a debris flow fan in Kamikamihori Valley, near Mt. Yakedake, Japan. During a twelve year study, the researchers documented one shift in the active channel. They attributed the change in position to a channel blockage located at the upper end of the first channel (Suwa and Okuda, 1983). Various researchers have proposed that fan-head-trenching is

responsible for the lateral growth of debris flow fans (Hooke, 1967; Harvey, 1984; Blair and McPherson, 1994; Dühnforth et al., 2007; Wasklewicz and Scheinert, 2016). Fan-head-trenching is caused by fan incision. That process causes debris flow deposition to shift toward mid- and distal-fan regions. Trenching can lead to the formation of new depositional lobes, which form at the distal edge of old fan segments. In these cases, sediment is no longer deposited on older fan surfaces (Hooke, 1967; Harvey, 1984; Blair and McPherson, 1994; Dühnforth et al., 2007; Wasklewicz and Scheinert, 2016).

A debris flow fan growth model was conceptualized from field observations in Yosemite Valley. It should be noted that fan-head-trenching is not visible at any of the field sites. If trenching were present, debris flow fans would be composed of multiple depositional lobes and not a single lobe. The first two phases of the model, proposed below, are in agreement with the process of fan construction proposed by Beaty (1963, 1970) and Hooke (1967). Fan growth can be described by three phases: fan base development, vertical growth, and lateral growth. The first phase of growth is in the horizontal direction, where consecutive debris flows form the fan base. Mapping of levees at each study site reveals that the position and course of debris flows change through time. Channel switching is likely caused by large blockages and obstructions. During the passage of a debris flow, these channel obstructions deflect the debris flow laterally. The model predicts that the fan base is constructed through a series of flow deflections, where flows spread out, forming the initial fan footprint (Fig. 22).

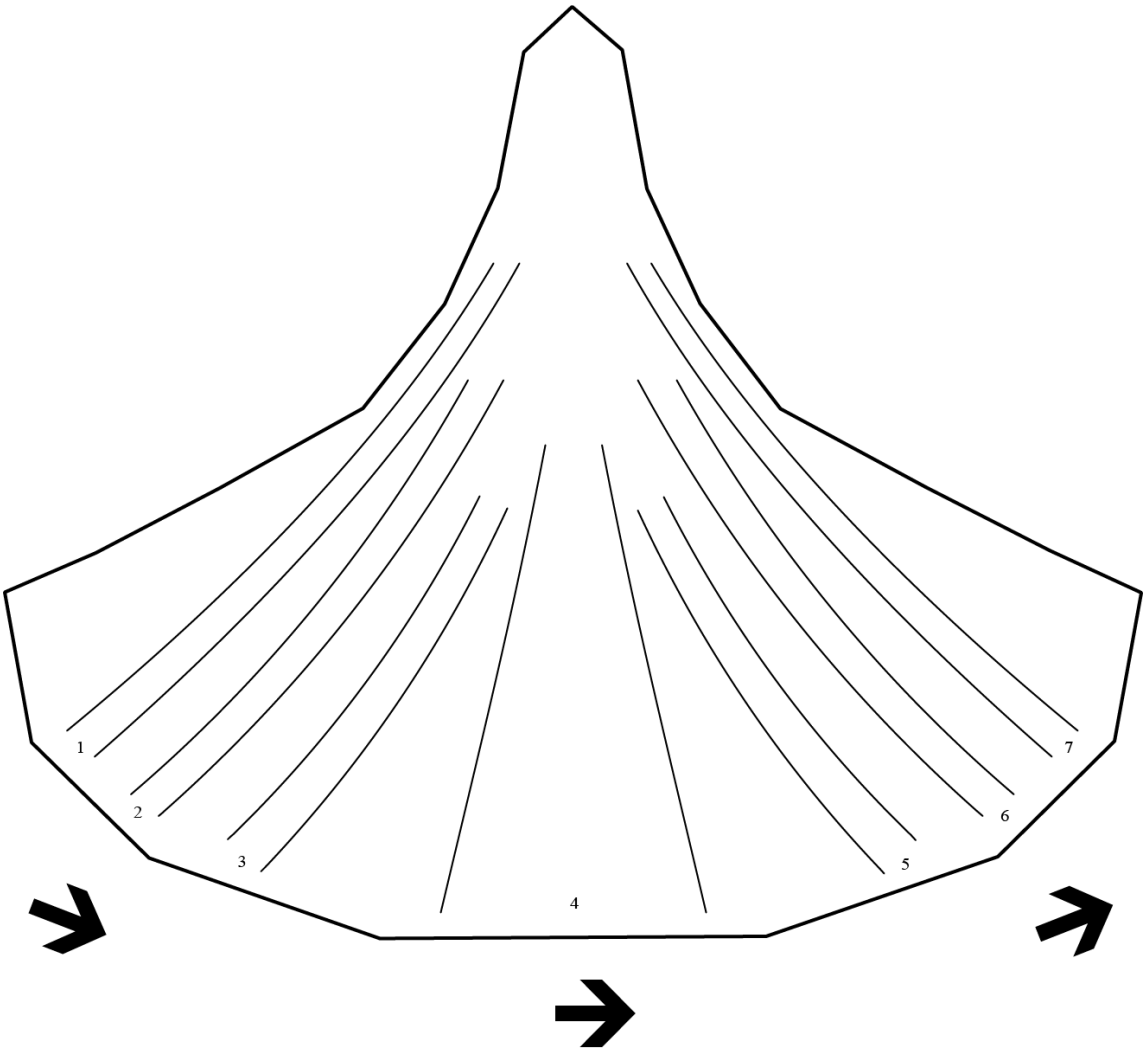

Figure 22. First phase of the fan growth model (aerial view). The figure represents how successive debris flows (1-7) spread out to form the fan base.

In the second phase of the growth model, a fan aggrades vertically due to episodes of resurfacing. Resurfacing occurs when flow deflections cause debris flows to be deposited back and forth across the fan surface (Fig. 23). Eventually, the fan aggrades vertically and reaches a steady state slope.

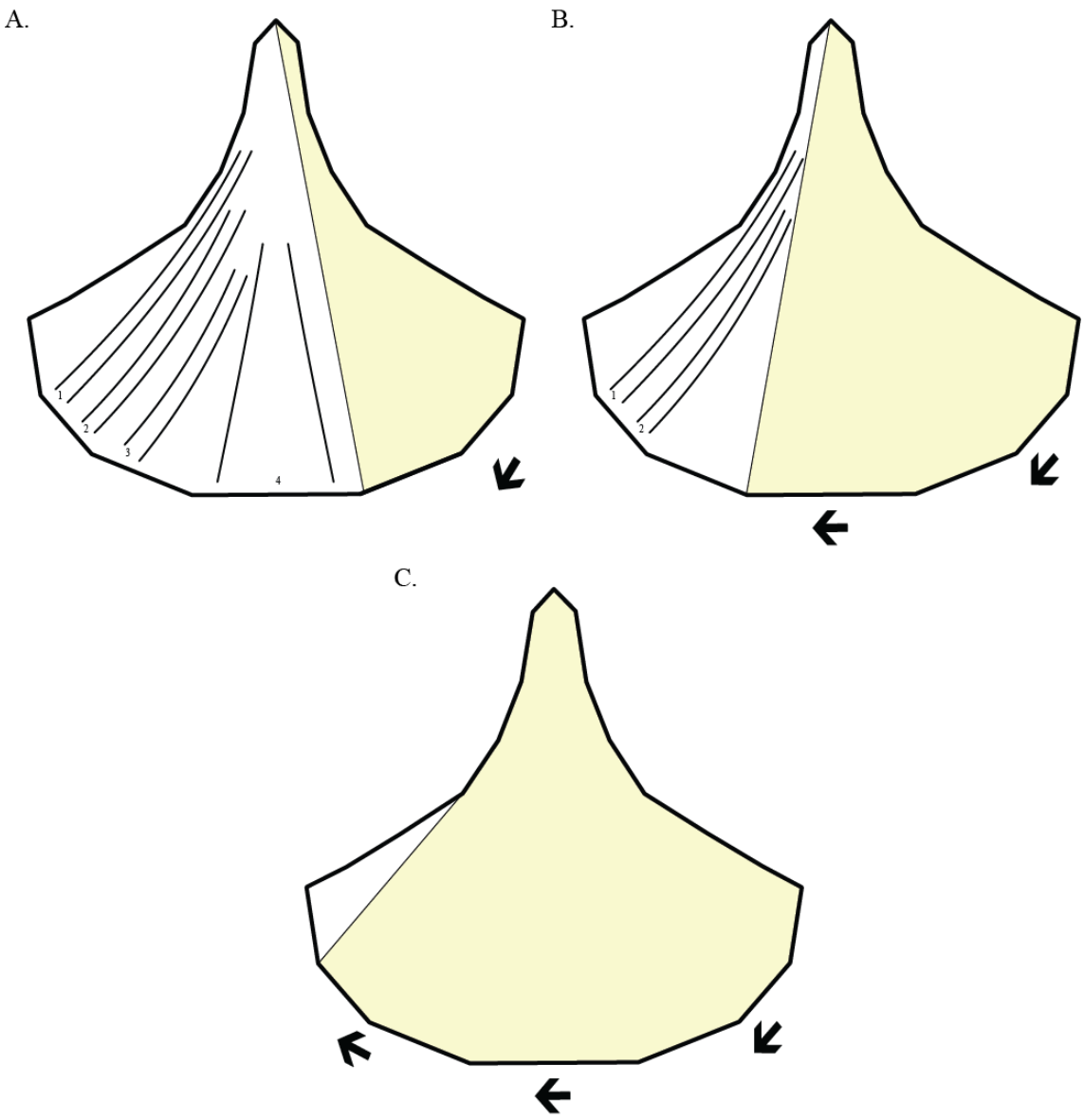

Figure 23. Second phase of fan growth model (aerial view). The tan polygons represent debris flow deposition following fan base development. Steps A-C show how debris flow deflection causes fan resurfacing.

In the third phase of the growth model, the fan grows laterally, maintaining a steady state slope. The slope angle is controlled by debris flow rheology, where flows with higher yield strength deposit fans with steeper slopes than flows with lower yield strength.

Future resurfacing events cause the fan to grow laterally through vertical accretion (Fig. 24). The third step of this model explains how a fan grows laterally when fan-head-trenching is not present.

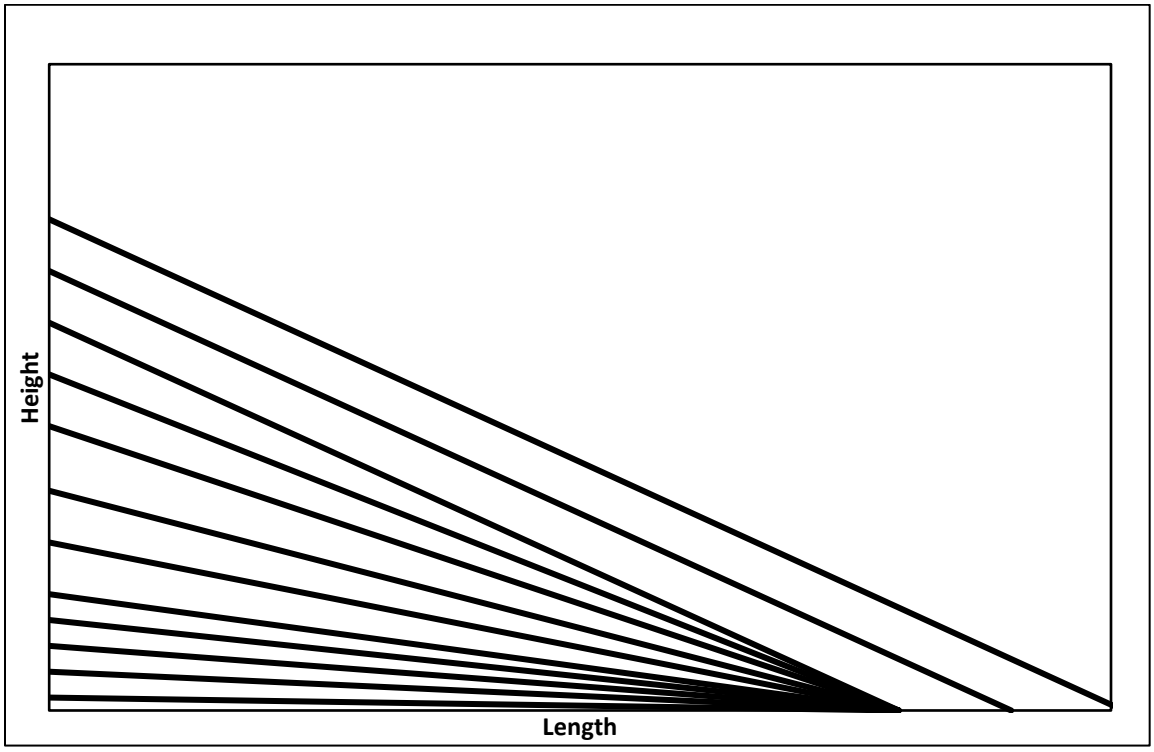

Figure 24. Third phase of fan growth (cross-sectional view). At this stage of growth, any resurfacing causes the fan to prograde at a constant slope through vertical accretion.

Debris Flow Risk Assessment in Yosemite Valley

Yosemite Valley has been the site of large and potentially dangerous debris flows. These prehistoric events are recorded by bouldery levees that are deposited on the surface of each fan. The volume of material that was transported by a debris flow can quantify the magnitude of a single event. The largest debris flow recorded by the study was found on the Indian Creek Fan and had an estimated volume of 64,587 m^3. Large debris flows pose a potential threat to the infrastructure, inhabitants, and visitors of Yosemite Valley.

Future debris flow initiation in Yosemite Valley is dependent on two factors: available sediment and sufficient water discharge. Field observations show that the active channels at Eagle Creek and Indian Creek are loaded with sediment. In addition, the Sentinel Creek talus pile has an abundance of loose sediment on its surface. Thus, high magnitude rainfall is all that is needed to mobilize sediment along each channel. For this reason, there is the high potential for loss of life and damage to infrastructure in Yosemite Valley when the right conditions are present.

CONCLUSIONS

Data were collected at three fans in Yosemite Valley to assess the potential debris flow hazards in the valley. DGPS receivers were used to map debris flow levees and the locations of sediment size analyses. Additionally, cosmogenic dating was used to date the youngest debris flow event along the Indian Creek fan. Grain size measurements of levees demonstrated that prehistoric debris flows were capable of transporting boulders ranging from 0.1-5.1 m in diameter into Yosemite Valley. Furthermore, cosmogenic dating at the Indian Creek fan indicates that the fan was quickly constructed by 12.1 ka. The timing of deposition at Indian Creek suggests that fans at Eagle Creek and Sentinel Creek were also constructed quickly after the LGM. It is hypothesized that a wetter climate during the Late Pleistocene provided sufficient water flow to transport available sediment into the valley. In addition, slope failure related to glacial debuttressing and weathering most likely provided the catchments in the study area with loose sediment. This research has also aided in conceptualizing a model of debris flow fan construction. The fan growth model describes fan construction in three phases: fan base development,

vertical growth, and lateral growth. More importantly the model proposes a mechanism of lateral growth, unrelated to fan-head-trenching. The active channels at Indian, Eagle, and Sentinel creeks are loaded with large volumes of sediment. At the present time, debris flow initiation in Yosemite Valley is dependent on high water flows. Debris flows pose a significant hazard to Yosemite Valley, if and when, the optimum conditions are met.

REFERENCES CITED

Anderson, R.S., and Carpenter, S.L., 1991, Vegetation change in Yosemite Valley, Yosemite National Park, California, during the Protohistoric period: Madroño, v. 38, p. 1-13.

Ballantyne, C.K., 2002, A general model of paraglacial landscape response: The Holocene, v.12, p. 371-376.

Ballantyne, C.K., and Stone, J.O., 2004, The Beinn Alligin rock avalanche, nw Scotland: Cosmogenic 10Be dating, interpolation, and significance: The Holocene, v. 14, p. 448-453.

Bateman, P.C., 1992, Plutonism in the Central Part of the Sierra Nevada Batholith, California: United States Geological Survey Professional Paper 1483, 185 p.

Bateman, P.C., and Wahrhaftig C., 1966, Geology of the Sierra Nevada, *in* Bailey, E.H., eds., Geology of Northern California: Sacramento, California Division of Mines and Geology Bulletin, v. 190, p. 107-172.

Beaty C.B., 1963, Origin of alluvial fans, White Mountains, California and Nevada: Association of American Geographers Annals, v. 53, p. 516-555.

Beaty, C.B., 1970, Age and estimated rate of accumulation of an alluvial fan, White Mountains, California, U.S.A.: American Journal of Science, v. 268, p. 50-77.

Blair, T.C., and McPherson, J.G., 1994, Alluvial fan processes and forms, *in* Parsons, A.J., eds., Geomorphology of dessert environments, London, Chapman and Hall, p. 354-402.

Brody, A.G., Pluhar, C.J., Stock, G.M., and Greenwood, J.W., 2015, Near-surface geophysical imaging of a talus deposit in Yosemite Valley, California: Environmental and Engineering Geoscience, v. 21, p. 111-127.

Bull, W.B., 1964, Alluvial fans and near-surface subsidence in western Fresno County, California: United States Geological Survey Professional Paper 352-E, 71 p.

Bull, W.B., 1977, The alluvial fan environment: Progress in Physical Geography, v.1, p. 222-270.

Burgess, S.D., Bowring, S.A., Petsche, J., Miller, R.B., and Miller, J.S., 2009, High Precision U-Pb CA-TIMS Geochronology for the Sentinel and Yosemite Creek Granodiorites, Sierra Nevada Batholith, CA: A history of punctuated intrusion and protracted crystallization: Abstract V42A-05 presented at 2009 Fall Meeting, AGU, San Francisco, California, 14–18 December.

Calkins, F.C., 1985, Bedrock geologic map of Yosemite Valley National Park, California: United States Geological Survey, scale 1:24,000.

Church, M., and Ryder, J.M., 1972, Paraglacial sedimentation: A consideration of fluvial processes conditioned by glaciation: Geological Society of America Bulletin, v.83, p. 3059-3072.

Cossart, E., Braucher, R., Fort, M., Bourlès, D.L., and Carcaillet, J., 2008, Slope instability in relation to glacial debuttressing in alpine areas (Upper Durance catchment, southeastern France): Evidence from field data and ^{10}Be cosmic ray exposure ages: Geomorphology, v. 95, p. 3-26.

Denny, C.S., 1967, Fans and pediments: American Journal of Science, v. 265, p. 81-105.

Dühnforth, M., Densmore, A.L., Ivy-Ochs, S., Allen, P.A., and Kubik, P.W., 2007, Timing and patterns of debris flow deposition on Shepherd and Symmes Creek fans, Owens Valley, California, deduced from cosmogenic ^{10}Be: Journal of Geophysical Research: Earth Surface, v. 112.

Ericson, K., Migoń, P., Olvmo, M., 2005, Fractures and drainage in the granite mountainous area: A study from Sierra Nevada, USA: Geomorphology, v. 64, p. 97-116.

Evans, S.G., and Clague, J.J., 1994, Recent climatic change and catastrophic geomorphic processes in mountain environments: Geomorphology, v. 10, p. 107-128.

Gabet, E.J., and Bookter, A., 2008, A morphometric analysis of gullies scoured by post-fire progressively bulked debris flows in southwest Montana, USA: Geomorphology, v. 96, p. 298-309.

Harvey, A.M., 1984, Aggradation and dissection sequences on Spanish alluvial fans: Influence on morphological development: Catena, v. 11, p. 289-304.

Hidy, A.J., Gosse, J.C., Froese, D.G., Bond, J.D., and Rood, D.H., 2013, A latest Pliocene age for the earliest and most extensive Cordilleran ice sheet in northwest Canada: Quaternary Science Review, v. 61, p. 77-84.

Hooke, R.L., 1967, Processes on arid-region alluvial fans: Geology, v.75, p. 438-460.

Hooke, R.L., and Rohrer, W.L., 1979, Geometry of alluvial fans: Effect on discharge and sediment size: Earth Surface Processes and Landforms, v. 4, p. 147-166.

Johnson, A.M., and Rodine, J.D., 1984, Debris Flow, *in* Brunsden, D., and Prior, D.B. eds., Slope Instability: New York, Wiley and Sons, p. 257-361.

Johnson, C.G., Kokelaar B.P., Iverson R.M., Logan, M., LaHusen, R.G., and Gray, J.M.N.T., 2012, Grain-size segregation and levee formation in geophysical mass flows: Journal of Geophysical Research: Earth Surface, v.117.

Larsen, I.J., Pederson, J.L., and Schmidt, J.C., 2006, Geologic versus wildfire controls on hillslope processes and debris flow initiation in the Green River canyons of Dinosaur National Monument: Geomorphology, v. 81, p. 114-127.

Major, J.J., and Iverson, R.M., 1999, Debris-flow deposition: Effects of pore-fluid pressure and friction concentrated at flow margins: Geological Society of America Bulletin, v. 111, p. 1424-1434.

Memeti, V., Paterson, S., Matzel, J., Mundil, R., and Okaya, D., 2010, Magmatic lobes as "snapshots" of magma chamber growth and evolution in large, composite batholiths: An example from the Tuolumne intrusion, Sierra Nevada, California: Geological Society of America Bulletin, v.122, p. 1912-1931.

Messing, S.A., 2001, Late-glacial and early Holocene vegetation and climate change near Owens Lake, eastern California: Quaternary Research, v. 55, p. 57-65.

Migoń, P., and Vieira, G., 2014, Granite geomorphology and it geologic controls, Serra da Estrela, Portugal: Geomorphology, v. 226, p. 1-14.

National Center for Airborne Laser Mapping, 2006, Filtered LiDAR DEM for Yosemite Valley: National Center for Airborne Laser Mapping dataset-1048555.

National Oceanic and Atmospheric Administration, 2012, Climatological Data Annual Summary: California dataset v.116.

National Park Service, 2012, Annual Park Visitation: https://irma.nps.gov/Stats/SSRSReports/Park Specific Reports/Annual Park Visitation (All Years)?Park=YOSE (April 2013).

Pye, K., 1986, Mineralogical and textural controls on the weathering of granitoid rocks: Catena, v. 13, p. 44-57.

Rood, D.H., Burbank, D.W., Finkel, R.C., 2011, Chronology of glaciation in the Sierra Nevada from ^{10}Be surface exposure dating: Quaternary Science Reviews, v.30, p. 646-661.

Schürch, P., Densmore, A.L., Rosser, N.J., and McArdell, B.W., 2011, Dynamic controls on erosion and deposition on debris flow fans: Geology, v. 39, p. 872-830.

Smith S.J., and Anderson R.S., 1992, Late Wisconsin paleoecological record from Swamp Lake, Yosemite National Park, California: Quaternary Research, v. 38, p. 91-102.

Stock, G.M., and Uhrhammer, R.A., 2010, Catastrophic rock avalanche 3600 years BP from El Capitan, Yosemite Valley, California: Earth surface processes and landforms, v. 35, p. 941-951.

Street, J.H., Anderson, R.S., and Paytan, A., 2012, An organic geochemical record of Sierra Nevada climate since the LGM from Swamp Lake, Yosemite: Quaternary Science Reviews, v. 40, p. 89-106.

Suwa, H., and Okuda, S., 1983: Deposition of debris flows on a fan surface, Mt. Yakedake, Japan: Zeitschrift fur Geomorphologie NF Supplementband, v. 46, p. 79-101.

Wasklewicz, T., and Scheinert, C., 2016, Development and maintenance of a telescoping debris flow fan in response to human-induced fan surface channelization, Chalk Creek Valley natural debris flow laboratory, Colorado, USA: Geomorphology, v. 252, p. 51-65.

Whipple, K.X., and Dunne, T., 1992, The influence of debris-flow rheology on fan morphology: Geological Society of American Bulletin, v. 104, p. 887-900.

Wieczorek, G.F., and Jäger, S., 1996, Triggering mechanisms and depositional rates of postglacial slope-movement processes in the Yosemite Valley, California: Geomorphology, v. 15 p. 17-31.

Wieczorek, G.F., and Snyder, J.B., 2004, Historic Rock Fall in Yosemite Valley National Park, California: U.S. Geological Survey Open-File Report 03-491, 10 p.

APPENDIX A: Debris Flow Levee Metrics

Table A1

Indian Creek Levee Metrics					
Levee Cross Section ID	Width (m)	Height (m)	Area (m^2)	Length (m)	Volume (m^3)
1A-1	10	0.78	3.90		
1A-2	11	0.79	4.35		
1A-3	13	1.14	7.41		
1A-4	8	1.21	4.84		
1A-5	11	0.64	3.52		
1A Average			**4.80**	**123**	**591**
1B-1	14	2.00	14.00		
1B-2	13	1.00	6.50		
1B-3	15	1.00	7.50		
1B-4	10	1.00	5.00		
1B-5	10	1.00	5.00		
1B Average			**7.60**	**104**	**790**
1 Total:					**1381**
2A-1	9	0.50	2.25		
2A-2	14	0.50	3.50		
2A-3	10	0.86	4.30		
2A-4	18	0.96	8.64		
2A-5	14	0.59	4.13		
2A Average			**4.56**	**106**	**484**
2B-1	13	0.91	5.92		
2B-2	11	0.90	4.95		
2B-3	11	0.86	4.73		
2B-4	17	0.71	6.04		
2B-5	13	0.54	3.51		
2B Average			**5.03**	**76**	**382**
2 Total:					**866**

Table A1 (Cont.)

Indian Creek Levee Metrics					
Levee Cross Section ID	Width (m)	Height (m)	Area (m^2)	Length (m)	Volume (m^3)
3A-1	46	3.49	80.27		
3A-2	41	3.83	78.52		
3A-3	45	3.99	89.78		
3A-4	57	4.59	130.82		
3A-5	54	4.54	122.58		
3A Average			**100.39**	**556**	**55817**
3B-1	10	0.98	4.90		
3B-2	13	3.64	23.66		
3B-3	15	1.82	13.65		
3B-4	14	2.21	15.47		
3B-5	19	2.23	21.19		
3B Average			**15.77**	**556**	**8770**
3 Total:					**64587**
Overall Average					**21979**

Table A2

Eagle Creek					
Levee Cross Section ID	Width (m)	Height (m)	Area (m^2)	Length (m)	Volume (m^3)
1A-1	13	1.36	8.84		
1A-2	16	0.91	7.28		
1A-3	17	2.33	19.81		
1A-4	13	3.48	22.62		
1A-5	12	1.31	7.86		
1A Average			**13.28**	**122**	**1620**
1B-1	17	1.77	15.05		
1B-2	19	2.55	24.23		
1B-3	20	2.24	22.40		
1B-4	19	2.85	27.08		
1B-5	15	1.77	13.28		
1B Average			**20.40**	**222**	**4530**
1 Total:					**6150**
2A-1	22	2.77	30.47		
2A-2	26	2.60	33.80		
2A-3	36	2.93	52.74		
2A-4	22	2.01	22.11		
2A-5	22	2.30	25.30		
2A Average			**32.88**	**198**	**6511**
2B-1	10	1.87	9.35		
2B-2	22	2.88	31.68		
2B-3	15	1.41	10.58		
2B-4	15	2.15	16.13		
2B-5	14	2.14	14.98		
2B Average			**16.54**	**174**	**2878**
2 Total:					**9389**

Table A2 (Cont.)

Eagle Creek					
Levee Cross Section ID	Width (m)	Height (m)	Area (m^2)	Length (m)	Volume (m^3)
3A-1	20	3.13	31.30		
3A-2	24	2.66	31.92		
3A-3	27	3.17	42.80		
3A-4	15	2.16	16.20		
3A-5	15	0.52	3.90		
3A Average			**25.22**	**371**	**9358**
3B-1	12	2.21	13.26		
3B-2	25	4.01	50.13		
3B-3	10	1.92	9.60		
3B-4	22	2.76	30.36		
3B-5	15	1.08	8.10		
3B Average			**22.29**	**218**	**4859**
3 Total:					**14217**
4A-1	18	3.59	32.31		
4A-2	14	2.66	18.62		
4A-3	22	1.57	17.27		
4A-4	21	2.51	26.36		
4A-5	23	1.49	17.14		
4A Average			**22.34**	**240**	**5361**
4B-1	9	1.51	6.80		
4B-2	12	2.46	14.76		
4B-3	16	2.98	23.84		
4B-4	17	1.12	9.52		
4B-5	9	1.31	5.90		
4B Average			**12.16**	**71**	**864**
4 Total:					**6225**

Table A2 (Cont.)

Eagle Creek					
Levee Cross Section ID	Width (m)	Height (m)	Area (m^2)	Length (m)	Volume (m^3)
5A-2	17	2.36	20.06		
5A-3	13	1.19	7.74		
5A-4	9	1.02	4.59		
5A-5	13	0.57	3.71		
5A Average			**9.02**	**85**	**767**
5B-1	11	1.14	6.27		
5B-2	12	1.04	6.24		
5B-3	12	1.33	7.98		
5B-4	17	0.77	6.55		
5B-5	5	0.38	0.95		
5B Average			**5.60**	**53**	**297**
5 Total:					**1064**
6A-1	15	1.36	10.20		
6A-2	14	1.83	12.81		
6A-3	12	1.98	11.88		
6A-4	12	1.98	11.88		
6A-5	10	0.92	4.60		
6A Average			**10.27**	**85**	**873**
6B-1	15	1.25	9.38		
6B-2	18	2.21	19.89		
6B-3	18	1.77	15.93		
6B-4	17	1.08	9.18		
6B-5	12	0.58	3.48		
6B Average			**11.57**	**83**	**960**
6 Total:					**1834**

Table A2 (Cont.)

Eagle Creek					
Levee Cross Section ID	Width (m)	Height (m)	Area (m^2)	Length (m)	Volume (m^3)
7A-1	21	5.22	54.81		
7A-2	16	4.73	37.84		
7A-3	19	4.70	44.65		
7A-4	14	3.98	27.86		
7A-5	24	3.09	37.08		
7A Average			**40.45**	**296**	**11973**
7B-1	10	1.52	7.60		
7B-2	12	3.36	20.16		
7B-3	11	4.16	22.88		
7B-4	13	1.52	9.88		
7B-5	10	2.23	11.15		
7B Average			**14.33**	**319**	**4573**
7 Total:					**16545**
Overall Average					**7918**

Table A3

Sentinel Creek					
Levee Cross Section ID	Width (m)	Height (m)	Area (m^2)	Length (m)	Volume (m^3)
1A-1	24	2.74	32.88		
1A-2	26	2.65	34.45		
1A-3	25	1.77	22.13		
1A-4	37	0.96	17.76		
1A-5	22	0.49	5.39		
1A Average			**22.52**	**428**	**9639**
1B-1	26	2.20	28.60		
1B-2	26	2.08	27.04		
1B-3	18	2.55	22.95		
1B-4	24	2.11	25.32		
1B-5	12	1.00	6.00		
1B Average			**21.98**	**444**	**9760**
1 Total:					**19399**
2A-1	15	2.66	19.95		
2A-2	8	1.25	5.00		
2A-3	7	2.02	7.07		
2A-4	7	1.25	4.38		
2A-5	15	2.51	18.83		
2A Average			**11.04**	**206**	**2275**
2B-1	19	3.36	31.92		
2B-2	14	1.58	11.06		
2B-3	13	4.94	32.11		
2B-4	29	2.08	30.16		
2B-5	14	0.82	5.74		
2B Average			**22.20**	**148**	**3285**
2 Total:					**5560**

Table A3 (Cont.)

Sentinel Creek					
Levee Cross Section ID	Width (m)	Height (m)	Area (m^2)	Length (m)	Volume (m^3)
3A-1	16	3.99	31.92		
3A-2	13	3.10	20.15		
3A-3	17	2.52	21.42		
3A-4	15	1.89	14.18		
3A-5	17	1.54	13.09		
3A Average			**20.15**	**138**	**2781**
3B-1	21	4.69	49.25		
3B-2	37	4.51	83.44		
3B-3	31	4.60	71.30		
3B-4	20	1.61	16.10		
3B-5	33	2.29	37.79		
3B Average			**51.57**	**140**	**7220**
3 Total:					**10001**
4A-1	15	2.02	15.15		
4A-2	25	3.22	40.25		
4A-3	21	1.70	17.85		
4A-4	19	1.47	13.97		
4A-5	16	1.03	8.24		
4A Average			**19.09**	**150**	**2864**
4B-1	22	1.16	12.76		
4B-2	22	2.76	30.36		
4B-3	18	3.05	27.45		
4B-4	19	3.13	29.74		
4B-5	30	2.36	35.40		
4B Average			**27.14**	**199**	**5401**
4 Total:					**8265**

Table A3 (Cont.)

Sentinel Creek					
Levee Cross Section ID	Width (m)	Height (m)	Area (m^2)	Length (m)	Volume (m^3)
5A-1	28	8.36	117.04		
5A-2	17	6.12	52.02		
5A-3	20	5.06	50.60		
5A-4	29	4.62	66.99		
5A-5	17	3.58	30.43		
5A Average			**63.42**	**127**	**8054**
5B-1	27	8.50	114.75		
5B-2	31	13.09	202.90		
5B-3	35	5.69	99.58		
5B-4	22	2.44	26.84		
5B-5	17	0.78	6.63		
5B Average			**90.14**	**119**	**10726**
5 Total:					**18780**
Overall Average					**10334**

APPENDIX B: Average Debris Flow Widths and Lengths

Table B1

Indian Creek		
Flow ID	Width (m)	Length (m)
1	16	
1	17	
1	21	
1	23	
1	18	
1 Average:	**19**	**114**
2	10	
2	10	
2 Average:	**10**	**91**
3	21	
3	17	
3	14	
3	16	
3	16	
3 Average:	**16.8**	**556**

Table B2

Eagle Creek		
Flow ID	Width (m)	Length (m)
1	13	
1	11	
1	24	
1	28	
1	31	
1 Average:	**21**	**172**
2	12	
2	15	
2	16	
2 Average:	**14**	**186**
3	46	
3	49	
3	42	
3	22	
3	14	
3 Average:	**35**	**295**
4	20	
4	17	
4	26	
4	39	
4	41	
4 Average:	**29**	**156**
5	15	
5	15	
5	20	
5	22	
5	25	
5 Average:	**19**	**69**

Table B2 (Cont.)

Eagle Creek		
Flow ID	Width (m)	Length (m)
6	20	
6	15	
6	14	
6	18	
6	19	
6 Average:	**17**	**84**
7	34	
7	11	
7	10	
7	15	
7	13	
7 Average:	**17**	**308**

Table B3

Sentinel Creek		
Flow ID	Width (m)	Length (m)
1	30	
1	24	
1	20	
1	14	
1	16	
1 Average:	**21**	**436**
2	31	
2	20	
2	9	
2	19	
2	42	
2	27	
2 Average:	**23**	**177**
3	38	
3	40	
3	38	
3	31	
3	26	
3 Average:	**35**	**139**
4	30	
4	18	
4	16	
4	19	
4	24	
4 Average:	**21**	**175**
5	13	
5	12	
5	11	
5	12	
5	13	
5 Average:	**12**	**123**

APPENDIX C: D50, D90, and Dmax Values

Table C1

Indian Creek				
Longitude	Latitude	D50 (m)	D90 (m)	Dmax (m)
-119.5840996	37.75035846	0.72	1.87	4.64
-119.5841802	37.75089939	0.77	1.35	1.71
-119.5835197	37.74987989	0.57	0.98	1.50
-119.5836751	37.74988912	0.76	1.48	1.92
-119.5831043	37.75475969	1.06	2.60	2.90
-119.5832747	37.75480288	0.84	1.58	1.95
-119.5838664	37.75004068	0.70	1.20	2.40
-119.5840802	37.74981561	0.46	0.68	0.97
-119.5854611	37.75123244	0.59	1.00	1.60
-119.5843257	37.7501851	0.78	1.28	5.11
-119.5842495	37.74951154	0.68	1.24	3.00
-119.5841024	37.74867436	0.43	0.89	1.25
-119.5843711	37.74958707	0.58	1.19	1.79
-119.5856445	37.75099816	0.62	1.36	1.38
Average:		**0.68**	**1.34**	**2.29**

Table C2

Eagle Creek				
Longitude	Latitude	D50 (m)	D90 (m)	Dmax (m)
-119.6158227	37.73026579	0.75	2.39	3.50
-119.6160469	37.72837423	0.76	0.86	0.87
-119.6148545	37.72880748	0.64	1.02	1.72
-119.6162662	37.73193518	1.23	2.30	4.00
-119.6167531	37.73167072	0.89	2.15	4.00
-119.6161956	37.72839592	0.48	0.80	1.08
-119.6169594	37.72903438	0.74	1.97	2.00
-119.6169904	37.73081152	0.59	0.89	1.53
-119.6167878	37.73047887	0.80	1.36	1.56
-119.6169114	37.73200406	1.16	1.80	2.10
-119.6186054	37.72978904	0.99	1.32	1.34
-119.617154	37.73132346	1.09	2.44	2.82
-119.6172661	37.73140402	0.47	1.15	1.37
-119.6179904	37.73051353	0.81	1.55	1.67
-119.6133993	37.73136942	0.63	0.86	1.16
-119.614293	37.73165632	0.41	1.21	1.63
-119.6132023	37.731505	0.47	1.04	1.10
-119.6140789	37.73176662	0.58	1.05	1.14
-119.6159257	37.73160837	0.97	1.70	2.20
-119.6139573	37.73020817	0.78	1.04	1.49
-119.6167439	37.73301234	0.78	1.52	5.00
-119.6144116	37.73156155	0.50	0.89	1.73
-119.6154898	37.73178598	0.43	0.66	1.03
-119.6152958	37.73121574	0.56	0.92	0.94
-119.6151902	37.7315867	0.41	2.13	2.80
-119.6140323	37.73140377	0.73	1.11	1.16
-119.6151402	37.7315277	0.40	1.30	2.13
-119.6141968	37.73064228	0.80	1.57	2.60
-119.6141123	37.73135825	0.46	0.66	1.18
-119.613684	37.73102181	0.44	0.70	0.83
-119.61445	37.73127422	0.63	1.36	1.49
-119.6136898	37.73084987	0.37	0.56	0.69
-119.614417	37.73188685	0.98	1.43	2.42
-119.6169588	37.73394855	0.43	1.83	1.83
Average:		**0.68**	**1.34**	**1.89**

Table C3

Sentinel Creek				
Longitude	Latitude	D50 (m)	D90 (m)	Dmax (m)
-119.6029572	37.73142224	0.27	0.51	0.64
-119.6030737	37.73090466	0.35	0.93	1.45
-119.6038928	37.7313987	0.78	1.05	1.29
-119.6040533	37.73115165	0.32	0.47	1.10
-119.6039574	37.73003852	0.33	0.51	0.54
-119.6042957	37.72995667	0.43	1.16	1.35
-119.6031563	37.73033431	0.36	0.70	1.17
-119.6034515	37.72999129	0.57	1.14	1.48
-119.6030722	37.72997484	0.40	0.64	1.15
-119.6026272	37.72965019	0.80	1.24	1.48
-119.602316	37.72978524	0.36	0.51	0.78
-119.6025733	37.72951505	0.35	0.85	1.30
-119.6025437	37.72959377	0.25	1.20	1.30
-119.6023637	37.72940198	0.43	0.81	1.43
-119.6024459	37.72943365	0.39	1.05	1.70
-119.602329	37.72915554	0.41	0.90	1.06
Average:		**0.43**	**0.85**	**1.20**